



Planetary geomorphology

Susan J. Conway

► To cite this version:

Susan J. Conway. Planetary geomorphology. T.P. Burt; A.S. Goudie; H.A. Viles. The History of the Study of Landforms or the Development of Geomorphology: Volume 5: Geomorphology in the Second Half of the Twentieth Century, 58, Geological Society of London, pp.395 - 414, 2022, GSL Memoirs, 10.1144/M58-2021-33 . insu-03813767

HAL Id: insu-03813767

<https://insu.hal.science/insu-03813767>

Submitted on 13 Oct 2022

HAL is a multi-disciplinary open access archive for the deposit and dissemination of scientific research documents, whether they are published or not. The documents may come from teaching and research institutions in France or abroad, or from public or private research centers.

L'archive ouverte pluridisciplinaire **HAL**, est destinée au dépôt et à la diffusion de documents scientifiques de niveau recherche, publiés ou non, émanant des établissements d'enseignement et de recherche français ou étrangers, des laboratoires publics ou privés.

1 History of the Study of Landforms Volume 5: Geomorphology in the
2 Second Half of the Twentieth Century

3 Section C: Advances in research on processes and landforms

4 Chapter 25: Planetary geomorphology

5
6 Susan J. Conway

7 Nantes Université, Université d'Angers, Le Mans Université, CNRS UMR 6112 Laboratoire de
8 Planétologie et Géosciences, France

9 **Abstract**

10 With the advent of the space age, planetary geomorphology has become a stand-alone discipline.
11 This contribution provides a summary of the different processes that have been identified to form
12 landscapes and landforms on planetary bodies in our Solar System, including rocky planets, icy
13 planets and moons, dwarf planets, comets and asteroids. I highlight the insights these landforms
14 have provided into the workings of these bodies and how what has been learnt in space has often
15 taught us new lessons about the Earth. Finally, I conclude that despite the limitations imposed by
16 remote sensing, planetary geomorphology has a bright future in planning future missions to explore
17 our Solar System as well as understanding the data that will be returned.

18 **1 Introduction**

19 This chapter is rather different from the rest of those in this book. First it is the only one that takes us
20 away from our own planet. Secondly, it deals with a topic that was not covered, for obvious historical
21 reasons, in the four previous volumes of the History of the Study of Landforms. Thirdly, it does not
22 restrict itself to the temporal span of 1965-2000 which is the focus of this book. It reviews progress in
23 the study of planetary geomorphology up until the present and shows the progress that has been
24 made since the first successful missions were carried out from the mid-1960s onwards - It was in
25 1965 that Mariner 4 brought us back the first close-up photographs of another planet: Mars.

26 Planetary geomorphology is a branch of planetary science, which was born in the second half of the
27 Twentieth Century from astronomy and has foundations in geology, meteorology, chemistry and
28 biology. The rise of planetary geomorphology as a discipline goes hand in hand with an increasing use
29 of satellite remote sensing data to study our own planet and the associated development of
30 techniques to exploit these data.

31 The first remote sensing image of the Earth taken from space was in 1946. Only twenty years later,
32 the NASA Mariner missions marked the first of a flurry of space missions that have only increased in
33 number as the century progressed, bringing us images, topography and other data from all the major
34 bodies in the Solar System and more. The objective of this chapter is not to provide a history of space
35 exploration, which is done elsewhere (e.g., Burns, 2010), but to highlight the main discoveries and
36 associated advances in the understanding of the processes and landforms of other worlds spanning
37 the era of robotic and human exploration of space.

38 In order for landscapes and landforms to be studied the surface of the body has to be resolved at a
39 sufficient resolution (in the author's opinion at least hundreds of metres per pixel). Hence to date,
40 planetary geomorphology is restricted to solid bodies in our Solar System and relies on space probes
41 sent to or near to the body of interest. We therefore have geomorphological information on (listed in
42 approximate increasing solar distance):

- 43 • Mercury
- 44 • Venus*
- 45 • The Moon*
- 46 • Mars* and its moons Phobos and Deimos
- 47 • Dwarf planet Ceres in asteroid belt
- 48 • Asteroids (Bennu*, Ryugu *, Itokawa*, Vesta, Ida, Eros, Mathilde, Gaspra, Šteins, Toutatis)
- 49 • The satellites of Jupiter (Io, Europa, Ganymede, Callisto)
- 50 • The satellites of Saturn (Pan, Daphnis, Atlas, Prometheus, Pandora, Epimetheus, Janus,
51 Mimas, Enceladus, Tethys, Telesto, Calypso, Dione, Helene, Rhea, Titan*,Hyperion, Iapetus,
52 Phoebe)
- 53 • The satellites of Neptune (Proteus, Triton)
- 54 • The satellites of Uranus (Miranda, Ariel, Umbriel, Titania, Oberon)
- 55 • Dwarf planet Pluto and its moon Charon
- 56 • Trans-Neptunian Kuiper belt object "Arrokoth"
- 57 • Comets (Tempel 1*, Churyumov–Gerasimenko 67P*, Borrelly, Wild 2, Hartley 2)

58 (A * symbol indicates a landed mission)

59 This exploration has revealed a suite of familiar and unfamiliar processes and landforms compared to
60 those found on Earth. This review will consider first processes and landforms already known from
61 studying the Earth before the space exploration era and then move towards those processes and
62 landforms less studied before Planetary Geomorphology became a distinct subdiscipline. Each
63 section will highlight lesser-known landforms and knowledge gained from studying other worlds. For
64 an exhaustive list of the landforms present on other worlds I refer the reader to the Encyclopaedia of
65 Planetary Landforms (Hargitai and Keresztsuri, 2015). For brevity only one or two references are cited
66 per topic, with the intent that an interested reader can use them to access to the wider relevant
67 literature on each topic.

68 2 Planetary aeolian landforms and processes

69 All bodies with an atmosphere have wind and aeolian landforms have been reported from: Mars,
70 Venus Titan and Pluto (Lorenz and Zimbelman, 2014; Telfer et al., 2018), as well as of course Earth.
71 For a full review of planetary aeolian landforms and associated processes I refer interested readers to
72 Bourke et al. (2019). The observation of aeolian bedforms including ripples, megaripples and dunes
73 on other planetary bodies (Figure 1a,b) has been very important for understanding the basic physics
74 underlying aeolian processes, because these planetary bodies provide different atmospheric
75 densities and particle densities spanning a wider range of parameter space than accessible on Earth
76 at the landscape-scale (Kok et al., 2012; Lapôtre et al., 2020). Martian aeolian bedforms have a wider
77 diversity of form and size than their terrestrial equivalents (e.g., Bourke, 2010; Sullivan et al., 2020),
78 which has led to researchers to question whether the basic physics underlying their formation are
79 indeed the same. A prime example is the landform called a Transverse Aeolian Ridge (Figure 1c)
80 which at < 1 m tall are thought to represent megaripples whose morphology is determined by
81 grainsize sorting rather than reptation and creep and whose origin remains unknown at larger

82 amplitudes (Zimbelman and Foroutan, 2020). Another example comes from radar images of
83 longitudinal parallel and occasionally bifurcating ridges have been interpreted to be longitudinal
84 dunes (Figure 1d) on Venus and Titan. Such dunes on Earth indicate strongly unimodal winds yet the
85 “physics of saltation on Titan and Venus is fundamentally different from that on Earth and Mars [...]”
86 dominated by direct fluid lifting” (Kok et al., 2012).

87 Hence, planetary observations have also revealed aeolian processes that are only experienced on
88 extra-terrestrial environments resulting in potentially unique landforms. These include bedforms
89 created by ablation (in the form of sublimation of ices – see also Section 11) rather than particle
90 movements (Bordiec et al., 2020), which have so far only been studied in detail on the Antarctic ice
91 cap (van den Broeke and Bintanja, 1995) or in ice caves (Obleitner and Spötl, 2011). Another
92 surprising result was the discovery of dunes on the comet 67P Churyumov–Gerasimenko, which has
93 no atmosphere (Jia et al., 2017; Thomas et al., 2015). These “dunes” are thought to form at times
94 when the comet is close to the sun causing vigorous outgassing and strong winds being setup
95 between sunlit and shadowed areas on the surface (Jia et al., 2017). Scouring “upwind” and build-up
96 of sediment on the “downwind” of boulders supports this hypothesis (Mottola et al., 2015).

97 Abrasion by particles lofted by the wind results in erosional aeolian landforms, such as yardangs and
98 the landscape-scale (Figure 1e) and ventifacts at the “field” scale (e.g., Wells and Zimbelman, 1997) –
99 the orientation of these landforms is used as an important indicator of prevailing wind directions.
100 Yardangs have been studied in most detail on Mars, but also have been suggested on Venus (Greeley
101 et al., 1995), Titan (Paillou et al., 2016) and as an alternative interpretation of the “dunes” on Pluto
102 (Moore et al., 2018). The study of yardangs on Mars drove a renaissance for their study on Earth
103 (Goudie, 2007) where their climate significance is still debated. Ventifacts have been observed at the
104 surface of Mars and are remarkably similar to those found on Earth (Knight, 2008; Laity and Bridges,
105 2009) and most modern studies of terrestrial ventifacts refer to planetary-driven research on this
106 topic.

107 Wind can also drive the formation of inverted landforms, which have been of particular importance
108 in revealing ancient fluvial processes on Mars (Davis et al., 2016; Day and Kocurek, 2016)(Section 3).
109 Wind is the agent that erodes and deflates the sediments surrounding the channel(s) which are more
110 resistant to abrasion (Figure 1e). This additional resistance can come about from cementation,
111 coarser grainsizes or lava capping (e.g., Williams et al., 2009).

112 Particular to Mars are landforms related to the copious dust at its surface, which also influences the
113 atmospheric circulation on that body (e.g., Madeleine et al., 2011). Dust via airfall is incorporated in
114 sedimentary deposits and ice-deposition landforms (e.g. the polar caps - Kieffer, 1990; or the ice-dust
115 latitude dependant mantle - Mustard et al., 2001). Unique to Mars are “Slope Streaks” which are
116 landforms associated with dust motion down steep slopes (e.g., Schorghofer et al., 2007; Sullivan et
117 al., 2001), see Section 7 for further details. Dust Devils are atmospheric vortices which are common
118 on Mars (Figure 1f) and have been observed by every landed mission (e.g., Ferri et al., 2003; Greeley
119 et al., 2006b; Ryan and Lucich, 1983; Thomas and Giersch, 1985). They can also be found in deserts
120 on Earth (Balme and Greeley, 2006), yet on Mars they often remove the dust on the surface leaving a
121 tortuous track in their wake which is clearly visible from orbit. Much recent research on terrestrial
122 dust devils has been driven by the desire to better understand the phenomenon on Mars (e.g., Balme
123 et al., 2012; Reiss et al., 2010).

124 3 Planetary fluvial landforms and processes

125 The possibility of extraterrestrial fluvial geomorphology was first revealed by the discovery of valley
126 networks and channel systems on the surface of Mars (Masursky, 1973) (Figure 2a). On Saturn's
127 satellite Titan fluvial landforms in the form of valley networks (Porco et al., 2005; Tomasko et al.,
128 2005) are thought to be formed by flowing liquid methane eroding the 'bedrock' of ice (Perron et al.,
129 2006) (Figure 2b). Together with the observation of lakes (see section 4), the existence of valley
130 networks on Titan has led to the hypothesis of a hydrocarbon-cycle driven by the decade-long
131 seasonal cycle and atmospheric synthesis of hydrocarbons. On Venus, the river-like canali could be
132 lava channels or carved by, another as-yet unidentified, fluid (Jones and Pickering, 2003; Kargel et al.,
133 1994; Komatsu and Baker, 1994). Equally dendritic valleys on Pluto have been proposed to be carved
134 by flowing liquid nitrogen (Stern et al., 2017) - the favoured alternate interpretation as glacial in
135 origin, is described in Section 8.

136 The observation of valley networks motivated the hypothesis that Mars had a full-hydrological cycle
137 early in its history, when its atmospheric density was higher allowing surface liquid water to be stable
138 (Baker et al., 1991; Pollack et al., 1987). This valley networks are visible in a degraded (Ansan et al.,
139 2008; Baker and Partridge, 1986) or inverted (Davis et al., 2016) state on the oldest visible surfaces of
140 Mars (Figure 2a). Some of these valleys have low tributary order/number and by analogy with valleys
141 with similar morphology on Earth have been interpreted to originate via groundwater sapping (Luo
142 and Howard, 2008), hence revealing the potential presence of aquifers, although this interpretation
143 has been questioned (Lapotre and Lamb, 2018). Some have also been interpreted to originate from
144 sub-icesheet drainage (Grau Galofre et al., 2020), attesting to potentially widespread glaciation early
145 in Mars' history (Fastook and Head, 2015). The observation of meandering channel belts on Mars
146 brought into question the hypothesis that vegetation was a prerequisite for developing meanders
147 early in Earth's history (Ielpi and Lapôtre, 2020).

148 Outflow channels on Mars – thought to represent colossal outbursts of water (Baker and Kochel,
149 1979) from pressurised aquifers (Marra et al., 2015) - reach hundreds of kilometres in width and
150 thousands in length (Figure 2c). They are characterised by streamlined obstacles and often multiple
151 terrace levels indicating several pulses of activity (Warner et al., 2009). The outflow channels often
152 originate at "Chaos Terrain" which also exists on Mercury (Rodriguez et al., 2020), Europa and Pluto
153 (Skjelne et al., 2021) (Figure 2d), and hence is not a landform directly connected to fluvial processes.
154 Chaos terrain is thought to form by the fracturing of a layer of crust sliding over a lower lubricated
155 layer (water in the case of Mars and Europa and glacial flow of N₂ ice for Pluto). Alternatively, such
156 outflow channels could be carved by very fluid lava (Leverington, 2011), as is thought to be the case
157 for analogous channels found on Mercury (Byrne et al., 2013).

158 Mars' surface hosts many enigmatic discontinuous channel segments, some of which have been
159 related to water release by impacts (Mangold, 2012). Others terminate in landforms that resemble
160 alluvial fans on Earth, such as Peace Vallis and its fan that was explored by the Curiosity Rover and
161 found to contain conglomerates (Williams et al., 2013). These observations, together with those of
162 the outflow channels point to surface water occurring only episodically, which contrasts with the
163 older valley networks which point to a full-hydrological cycle having existed on Mars. As surface
164 liquid water is not thought to have been stable for the last 1 Ga due to low atmospheric pressure and
165 humidity, all together this points to Mars's surface becoming more arid over time.

166 The smallest planetary landforms thought to be related to fluvial activity are kilometre-scale martian
167 gullies (Figure 2e) (Conway et al., 2019; Malin and Edgett, 2000) and the metres-wide and up to
168 hundreds of metres long Recurring Slope Lineae or "RSL" on Mars (Figure 2f) (McEwen et al., 2011).

169 Martian gullies resemble first-order drainage systems dominated by debris flow processes on Earth,
170 yet present-day flows in martian gullies during local winter argue against a completely fluvial origin
171 (Diniega et al., 2010; Dundas et al., 2019) – see Section 11. RSL are low albedo streaks that grow in
172 the hottest times of year extending from rocky steep slopes (Ojha et al., 2014) and have been
173 suggested to be water or brine seeps (Stillman et al., 2020), however the temporal and spatial limits
174 of orbital observations mean their origin remains enigmatic and could represent a uniquely martian
175 surface process and landform (F. Schmidt et al., 2017).

176 4 Coastal, lacustrine and karstic processes and landforms

177 Mars is the only planet besides Earth in the Solar System which is suspected to have had ocean-scale
178 open bodies of standing liquid (in this case water). Mars' valley networks and outflow channels
179 generally terminate in the northern lowlands and it is around these plains that two or more levels of
180 putative shorelines have been identified (Carr and Head, 2019; Parker et al., 1993). These shorelines
181 are characterised by a continuously traceable contact (expressed by albedo and/or topographic
182 contrasts - Figure 3a) over thousands of kilometres and interpreted to represent wavecut
183 platform(s). The lack of features typically associated with paleoshorelines on Earth, such as terraces,
184 or barrier ridges (Ghatan and Zimbelman, 2006; Malin and Edgett, 1999), means this interpretation
185 remains contentious. Variations in their altitude have been attributed to tectonic deformation post-
186 formation (Citron et al., 2018), and are also used as evidence against the landforms representing
187 shorelines (Sholes et al., 2021). The evidence for an ancient ocean is bolstered by the presence of
188 deltas whose altitudes are consistent with the ocean levels represented by the shorelines (Di Achille
189 and Hynek, 2010). Some of the shoreline landforms are alternately interpreted as the wash-up
190 deposits of tsunamis (Figure 3b) (Costard et al., 2017; Rodriguez et al., 2016), which also implies the
191 presence of an ocean.

192 Deltas are also one of the key lines of evidence in favour of the prevalence of paleolakes on ancient
193 Mars (Mangold et al., 2012) (Figure 3c). Other lines of evidence include sedimentary and in situ
194 observations by the Mars Science Laboratory rover Curiosity (Stein et al., 2018), spectral
195 observations from orbit (Dehouck et al., 2010), and morphological arguments – e.g., channels ingress
196 into depressions, but have no outlet or a higher elevation outlet (Cabrol and Grin, 1999; Fassett and
197 Head III, 2008; Goudge et al., 2016, 2015). The only other body in the Solar System thought to host
198 (or have hosted) seas or lakes is Saturn's Moon Titan (Figure 3d), whose 1.5 bar nitrogen-dominated
199 atmosphere and -180°C surface temperature means that liquid methane is believed to be the main
200 constituent of these lakes or seas, which are mainly located in polar regions. While some of these
201 bodies are connected to drainage systems, others are thought to be the result of karstic-type
202 dissolution processes (Mastrogiovanni et al., 2019). Deposits interpreted to be evaporitic associated
203 with basins located at Titan's tropics are inferred to be paleolakes or paleoseas (Moore and Howard,
204 2010), which could have resulted from seasonal (decadal timescales) or longer-term climatic changes
205 on Titan (MacKenzie et al., 2014).

206 Numerous sulphate salt deposits exist on Mars and hundred-metre-scale depressions within them
207 have been linked to karstic processes (Baioni and Sgavetti, 2013; Sefton-Nash et al., 2012) potentially
208 related to groundwater circulation (Grindrod and Balme, 2010). Dissolution has been invoked to
209 partly explain the collapse features associated with chaos terrain (described in Section 3).
210 Pseudokarst is where material is lost by mechanisms other than dissolution e.g. thermokarst, which
211 in a planetary context has been employed to describe karst-like features caused by temperature
212 induced volatile loss in contrast to the terrestrial definition which involves melting of ice-rich
213 permafrost. These karstic landforms are described further in Section 11 and martian thermokarst
214 initially also attributed to melting ice-rich permafrost are referred to in Section 8).

215 5 Planetary tectonic landforms and processes

216 Tectonic landforms are ubiquitous on planetary surfaces. Even the smallest bodies that have been
217 explored, such as comets, show signs of fracturing which result from interior forces (El-Maarry et al.,
218 2015). However, only the Earth has plate tectonics, whose action profoundly influences its
219 landscapes, making it one of the most dynamic surfaces in the Solar System. Europa, which is an icy
220 Moon of Jupiter, may have an analogous system of plates, but in this case the plates are made of
221 water ice floating on a liquid water “mantle” (Kattenhorn and Prockter, 2014) (Figure 4a). The
222 detailed morphology of Europa’s plates was key in motivating the dynamic modelling that underpins
223 our understanding of this planet’s interior. A similar “jostling plates” model has been advanced for
224 Venus based on analogy with deformational structures observed in actively deforming continents on
225 Earth (Byrne et al., 2021). Typical compressional tectonic landforms include wrinkle ridges, high relief
226 ridges and lobate scarps (Figure 4b, c), common on Mercury (Byrne et al., 2014), Mars (Herrero-Gil et
227 al., 2019; Nahm and Schultz, 2011), and the Moon (Schleicher et al., 2019; Watters et al., 2010). They
228 are thought to be compound landforms representing folds above faults, but not common on Earth
229 (Crane, 2020) hampering their interpretation. Global mapping these compressional tectonic features
230 on Mercury has provided an independent estimate of its global contraction (Byrne et al., 2014).

231 Typical extensional forms include graben (Figure 4d) and are found commonly throughout the solar
232 system. Graben systems are sometimes associated with pit-chains, which are thought to be caused
233 by fracture dilation (Ferrill et al., 2011) (Figure 4e) and whose origin is also interpreted to be
234 magmatic (see section 6):

235 Extensional tectonic features are very common on the icy moons of Jupiter, Saturn, and Neptune and
236 their patterns have been vital in understanding the forces that influence these bodies including tidal
237 stresses from their planets, crustal thickness, and mantle motions (Collins et al., 2009). Tectonic
238 landforms on these icy satellites can be unique, for example the double ridges on Europa (Figure 4a),
239 or the twisting double ridge-sets on Triton, or the prominent single equatorial ridge on Iapetus
240 (Figure 4f).

241 6 Planetary volcanic landforms and processes

242 The definition of volcanism has been extended beyond magmatic volcanism in a planetary science
243 context, to include also sedimentary volcanism and cryovolcanism and each are thought to produce
244 somewhat distinct landforms. Magmatic volcanism requires interior heating and an availability of
245 silicates to produce magma, so generally related volcanic landforms are found on terrestrial planets
246 of the inner solar system, as well as Earth’s Moon and Jupiter’s innermost moon Io. Volcanism at the
247 largest scale (hundreds to thousands of kilometres) is recognised in the form of volcanic constructs,
248 such as Tuilik Mons on Venus (Basilevsky et al., 2012) (Figure 5a) or Olympus Mons on Mars
249 (Morris, 1982) and/or volcanic plains, such as the Mare of the Moon (Figure 5b) (Stuart-Alexander
250 and Howard, 1970) or the Northern Plains of Mercury (Denevi et al., 2013). Peculiar to Venus are
251 coronae, arachnoids and novae, which are large patterns of fractures (concentric, concentric-radial
252 and radial, respectively) believed to be volcanic in origin (Head et al., 1992). Io is the only planetary
253 body in the Solar System where volcanic eruptions have actually been observed occurring (McEwen,
254 1998).

255 Recognisable at the kilometre to tens of kilometre-scale on Mars, the Moon, Venus and Io are
256 individual lava flows (Figure 5c – Io “dark flow”) and lava channels. On the Moon sinuous rilles
257 (Figure 5d) – sinuous channels hundreds of metres to kilometres in width and up to 500 km long -
258 were initially attributed to water (Peale et al., 1968), but are now generally acknowledged to be lava
259 channels carved predominantly by thermal erosion (Hurwitz et al., 2013). “Skylights” (Figure 5e) –

260 deep nearly vertically walled circular to elliptical depressions – on Mars and the Moon are
261 interpreted to represent the collapse of the roof of lava tubes and present considerable interest as
262 natural habitats which could be exploited for human exploration (Sauro et al., 2020). Larger pit
263 chains are thought to represent collapse on the withdrawal of lava from dikes (Wyrick, 2004) but
264 could also be tectonic in origin (see Section 5).

265 Evidence for explosive volcanism is usually smaller-scale (tens of kilometres) and more subtle in its
266 surface expression, taking the form of pits with associated red-colouration on Mercury (Kerber et al.,
267 2011) (Figure 5f), low-albedo markings on the Moon (Gustafson et al., 2012) and km-scale volcanic
268 cones on Mars (Brož and Hauber, 2012).

269 Sedimentary volcanism (often called mud volcanism) is driven by the circulation of water through a
270 planetary crust generally driven by tectonic forces or density contrasts and has been reported on
271 Mars (Figure 6a). Here, movement of groundwater is thought to have remobilised ancient
272 sedimentary deposits creating pitted cones and lobate-fronted flow features (Oehler and Allen,
273 2010). On Earth, mud volcanoes are the most commonly expressed landform resulting from
274 sedimentary volcanism and differ from their volcanic counterparts in terms of morphology, however
275 this distinction is harder to make on other bodies because of differences in environmental conditions
276 are difficult to directly infer the potential morphologic impacts (Brož et al., 2020).

277 Cryovolcanism is thought to be more abundant in the icy moons of the outer planets (Ahrens, 2020;
278 Kargel, 1995), where liquid water and ice, are thought to substitute almost directly the more familiar
279 lava and silicic rocks in the functioning of the volcanic plumbing system. On Ceres, brine driven
280 cryovolcanism is thought to explain the bright faculae, such as Cerealia Facula in Occator Crater
281 (Nathues et al., 2020) (Figure 6b). Inspired by planetary research cryovolcanic processes have been
282 cited as a potential cause for explosive pits that occurred in continuous permafrost on the Yamal
283 Peninsula in Russia (Buldovicz et al., 2018).

284 Diapirism (either compositional or thermal), where a less dense material rises through a denser one
285 above it is often associated with sedimentary- or cryo-volcanism. The resulting landforms can be a
286 result of tectonic deformation rather than extrusion at the surface. Several enigmatic terrains have
287 been attributed to diapirism or associated convection: the honeycomb and banded terrain in Hellas
288 basin on Mars (Figure 6c - cassis) (Bernhardt et al., 2016), Cantaloupe terrain on Triton (Schenk and
289 Jackson, 1993) or the cellular structure of Sputnik Planitia on Pluto (Howard et al., 2017b) (Figure 6d).

290 7 Mass movements on planetary bodies

291 Landslides have been identified on nearly every solid planetary surface observed in the solar system.
292 Notably the long runout landslides observed on bodies as diverse as Mars (Crosta et al., 2018;
293 McEwen, 1989), Mercury (Brunetti et al., 2015), the Moon (Boyce et al., 2020), Iapetus (Singer et al.,
294 2012), Callisto (Moore et al., 1999), Pluto's moon Charon (Beddingfield et al., 2020), Ceres (Duarte et
295 al., 2019) and Comet 67P (Lucchetti et al., 2019) (Figure 7a-c, landslide on Ceres, callisto moore et al,
296 Mars, Mercury) have inspired a comparative planetology approach seeking to understand the
297 physical processes underlying the motion of the long-runout landslides. The role that volatiles do or
298 do not play in the mobility of landslides is a key recurring theme. On one hand being used as an
299 argument to support inclusion of volatiles on Iapetus (Singer et al., 2012) and on the other being
300 used to refute their action on comet 67P (Lucchetti et al., 2019). For Ceres (Johnson and Sori, 2020;
301 B. E. Schmidt et al., 2017) as for Mars, both cases have been presented and no consensus has yet
302 been achieved (Harrison and Grimm, 2003; Johnson and Campbell, 2017).

303 Peculiar to Mars are a landform called “Slope Streaks” (Figure 7d) (Sullivan et al., 2001), which are
304 thought to represent avalanches of dust-sized material, taking the form of contrasting albedo,
305 downslope-widening streaks, up to several kilometres in length and hundreds of metres wide. Slope
306 Streaks usually appear as relatively dark (and sometimes relatively light) downslope oriented streaks
307 with barely detectable or negligible relief (Brusnikin et al., 2016; Chuang et al., 2007), which fade to
308 the background albedo over time. They often widen from a point source and can be sinuous,
309 overcome obstacles and have digitate margins. They can overtop small obstacles (Brusnikin et al.,
310 2016) yet are generally diverted by topographic irregularities (Miyamoto, 2004), so can form complex
311 bifurcating features. The involvement of liquid water has been invoked to explain their mobility on
312 low slopes (Bhardwaj et al., 2017), but dry granular mechanisms seem to also provide an adequate
313 explanation (Dundas, 2020).

314 Images at better than 1 m/pix on the Moon have revealed a diversity of mass movements on steep
315 slopes, including lobate and digitate dry granular flows on Moon (Figure 7e,f) (Senthil Kumar et al.,
316 2013; Xiao et al., 2013). The Moon and Mercury host unique surface textures hinting at slower
317 downslope movement of the surface regolith, including “elephant hide texture” on the Moon and
318 “chevron texture” on Mercury, whose precise origin is unknown (Zharkova et al., 2020). On Mars,
319 tens to hundreds of metre-scale lobate forms on slopes have been associated with the existence of a
320 solifluction-type movement on Mars (Gastineau et al., 2020; Johnsson et al., 2012) and are found in
321 association with other landforms interpreted to be periglacial in origin (see Section 8).

322 8 Planetary glacial and permafrost landforms and processes

323 Mars has an extensive suite of landforms at its mid-latitudes which are commonly accepted to be
324 debris covered glaciers (Figure 8a) dating from the last 1 Ga of Mars’ history. These glaciers can cover
325 tens to hundreds of kilometres and reach hundreds of metres thick. Their water ice core has been
326 revealed through orbital radar sounding (Petersen et al., 2018; Plaut et al., 2009), and their surface
327 textures indicate slow viscous deformation. Modelling studies (Karlsson et al., 2015; Parsons et al.,
328 2011) and the general lack of landforms associated with melt imply that the ice is likely perennially
329 frozen to the glacier bed (cold-based glaciers). The rare discovery of ridges interpreted to be eskers
330 connected to extant glaciers suggests that this constraint is only occasionally overcome (Butcher et
331 al., 2020; Gallagher and Balme, 2015). Isolated eskers and moraine-like ridges have been interpreted
332 to be signs of ancient glaciation and/or icesheets (Butcher et al., 2016; Head and Marchant, 2003).

333 On Pluto the existence of glaciers of N₂ ice has been reported (Howard et al., 2017a). These take the
334 form of smooth material filling topographic lows in highland terrains with longitudinal albedo
335 lineations indicating flow direction, which appear to flow out onto Sputnik Planum at lower elevation
336 where the lineations blend into the plains materials (Figure 8b). These glaciers are hundreds of
337 kilometres in length. The only other planetary body where debris covered glaciers have been
338 proposed is the dwarf planet Ceres (B. E. Schmidt et al., 2017), but their ambiguous morphology
339 means that landsliding could also be a viable interpretation.

340 Permafrost conditions exist on many bodies, particularly those in the outer solar system, yet
341 landforms typically associated with permafrost on Earth generally imply the degradation of ground
342 ice, or at least cycling of temperatures near water’s triple point to produce terrain modifications e.g.,
343 periglacial landforms. One exception is the formation of polygon crack patterns in ice-rich soil by
344 thermal contraction, which only requires temperature cycling – metre to decametre-scale examples
345 of these landforms have been widely reported at latitudes greater than 50°N and S on Mars
346 (Mangold, 2005; Mellon et al., 2009) where ground ice is thought to be prevalent (Feldman et al.,
347 2011). Periglacial landforms have been reported on Mars, implying the action of freeze-thaw cycling

348 in the planet's recent history and hence their interpretation as such remains a subject of debate.
349 These landforms include:

- 350 • Gullies, which are alcove-channel-fan systems hundreds of metres to kilometres in
351 length, which are found on steep slopes in the mid to high latitudes on Mars (Figure 2e)
352 (Harrison et al., 2015; Malin and Edgett, 2000). Their resemblance at landscape and
353 landform-scale to gullies carved by overland-flow and debris flow on Earth means that
354 they have been widely interpreted to form by these processes (Balme et al., 2006;
355 Conway and Balme, 2016; de Haas et al., 2015), and the source of water is likely from
356 snow and/or ground ice thaw. Yet their present activity has led to a re-evaluation of this
357 interpretation (see Section 11 - Sublimation landforms and processes).
- 358 • Surface albedo and/or clast patterns that resemble, and have a similar-scale to, sorted
359 patterned ground on Earth, including sorted circles on flat ground and stripes on sloping
360 terrain (Gallagher et al., 2011; Soare et al., 2016) (Figure 8c).
- 361 • Lobate forms interpreted to be solifluction lobes (see section 7) (Figure 8d).
- 362 • Polygonal patterned ground where the centres are lower than the margins and those
363 margins form double-ridges implying the existence of ice wedges (Soare et al., 2021,
364 2014) (Figure 8e).
- 365 • Scalloped depressions (Soare et al., 2008) and polygon junction pits (Costard et al., 2016)
366 were initially interpreted to be true thermokarst (i.e. caused by thaw). However,
367 together with expanded craters (Viola et al., 2015) are now thought to be caused by
368 sublimation (Dundas et al., 2015), see Section 11.
- 369 • Tens to hundreds of metre isolated hills or mounds with summit cracks/depressions
370 interpreted to be caused by ice-heave, otherwise known as "pingos" (Burr et al., 2009;
371 Soare et al., 2005) (Figure 8f).

372 9 Weathering

373 Weathering on planetary bodies produces regolith from rock via a range of breakdown processes,
374 some of them unknown on Earth. The landscape expression of these weathering processes includes
375 softening of primary landforms, such as impact craters, following a generally diffusive trend (Fassett
376 et al., 2017; Soderblom, 1970). Landforms directly linked to weathering processes, include regolith
377 surface textures and rock shapes, which tend to be expressed at the metre-scale or less. Hence, *in*
378 *situ* observations are best suited to inferring weathering processes are limited to the Moon, Mars,
379 asteroids Bennu and Ryugu and comet 67P.

380 On bodies without an atmosphere the surface is subject to a range of processes not experienced at
381 Earth's surface, including solar wind sputtering and micrometeorite impacts. In addition, thermal
382 stress and fatigue are greatly accentuated by the high amplitude thermal variations experienced on
383 many planetary surfaces compared to Earth (El Mir et al., 2019; Molaro and Byrne, 2012). Cracked
384 rocks or "Puzzle rocks" observed on Bennu (Walsh et al., 2019), Ryugu (Sasaki et al., 2021), the Moon
385 (Ruesch et al., 2020) and Mars (Eppes et al., 2015; Hötz et al., 1999) have been linked to thermal
386 fatigue and/or micrometeorite impacts (Figure 9a). On Mars rocks can also be sculpted by the wind –
387 producing ventifacts (Bridges et al., 1999; Greeley et al., 2006a; Thomson et al., 2008) (see also
388 Section 2). Pitted boulder surfaces on Mars have been linked to transient melting of snow (Head et
389 al., 2011) and volatile-related processes have been implicated in accelerating rock chute formation
390 (Levin et al., 2021) and boulder breakdown (de Haas et al., 2013).

391 A consequence of rock breakdown is rockfalls, which have been observed to occur in repeat imaging
392 of Mars (Grindrod et al., 2021; Vijayan et al., 2021) (Figure 9b). Roll/bounce marks left in the regolith

393 in the wake of boulders (Figure 9c) have shown rockfall to be a recently active process on the Moon
394 (Arvidson et al., 1975; Bickel et al., 2020). Patterns in the distribution of rockfall tracks have been
395 used to provide evidence for rock breakdown by thermal stress on Mars on the timescale of < 1 Ma
396 (Tesson et al., 2020), seismic activity on Mars (Roberts et al., 2012) and on the Moon (Senthil Kumar
397 et al., 2016), as well as inform the regolith strength on the Moon (Bickel and Kring, 2020).

398 Some puzzling aspects of surface regolith appearance have been attributed to surface sintering
399 caused by solar irradiation (Zharkova et al., 2020) (Figure 9d).

400 10 Impact Cratering

401 The process of impact cratering dominates most planetary surfaces apart from the Earth, Venus,
402 Titan and Io which either have dense atmospheres reducing the incoming impactor population
403 and/or surface processes that act to erase any crater landforms that are created. Impact craters
404 create topographic relief that can serve as a catalyst for other surface processes and they expose
405 materials from planetary interiors to active surface processes. For example, impacts can cause
406 substantial seismic shaking (Schultz and Gault, 1975) and therefore can initiate mass movements (see
407 Section 7).

408 The shape of an impact crater is primarily a function of the gravity, impactor size and the target
409 surface composition (Melosh, 1989). Other factors, such as impact speed and angle, impactor
410 composition, or target structure, also play a role in modulating the crater shape, but for the purposes
411 of this review will not be considered in further detail. With increasing impactor sizes craters evolve
412 from “simple” bowl-shapes towards more “complex”, including flat-floored with a central peak up to
413 multi-ringed basins (Figure 10a-c). The crater diameter at which the simple-to-complex transition
414 occurs varies from planetary body to planetary body and is traditionally represented by plotting the
415 population of craters on a logarithmic depth-diameter diagram. For example, on Mars the simple-to-
416 complex transition occurs at crater diameters of ~8 km, on Europa it occurs at ~1 km and Vesta at 28
417 km (Hiesinger et al., 2016).

418 Impact craters eject material from their cavity forming unique morphologies, such as ejecta blankets,
419 secondary crater clusters/chains, and visible radial “rays” which can be global in extent (Figure 10d).
420 Impact melt, found within the cavity and in the ejecta, shares many morphological characteristics
421 with lava and in ancient terrains on the Moon and Mercury, the distinction between them can be
422 challenging (Denevi et al., 2013). The outcrops located in crater walls and central peaks can provide
423 relatively fresh exposures of subsurface materials providing insights into the subsurface composition
424 of a body without having to drill *in situ* (Quantin et al., 2012).

425 Impact craters substantially disturb the crust (Kenkemann et al., 2014) and as a result can form a
426 structural conduit for endogenic processes that are then expressed at the surface, such as
427 hydrothermal circulation (Osinski et al., 2013), explosive volcanism (Thomas et al., 2014), or
428 cryovolcanism (Nathues et al., 2020).

429 Impact craters are used as an essential dating tool in planetary science, as their size-frequency
430 distribution is a function of the exposure age of a surface (Hartmann and Neukum, 2001). The
431 degradation state of the craters, hence the ability to recognise the surface processes that have
432 influenced them, is an important factor when interpreting the results of the crater size-frequency
433 distribution (Michael and Neukum, 2010).

434 **11 Sublimation landforms and processes**

435 Environments dominated by sublimation are rare on Earth, hence entire landforms or landscapes
436 dominated by this phase change are restricted to other planetary bodies. In particular the icy
437 satellites of the outer Solar System have surfaces dominated by various ices and whose sublimation
438 is thought to explain some of the most unusual landscapes (Mangold, 2011). For example, the entire
439 surface of Jupiter's moon Callisto is thought to have been extensively modified by the sublimation of
440 CO₂ and H₂O ices at its surface leaving a terrain dominated by dissected ridges and knobs (Figure 11a)
441 (White et al., 2016). Helene, in the Saturn system, has a sculpted surface attributed to remobilisation
442 of a thick layer of particles whose origin is sublimation from the plumes of Enceladus (Figure 11b)
443 (Hirata et al., 2014).

444 Comets are another planetary body where sublimation is the dominant landscape forming process
445 every time the comet approaches the sun. The first cometary orbital data from the Rosetta mission
446 to comet 67P revealed astonishingly diverse landscapes, including dunes (see Section 2), retreating
447 steep sided pits and cliffs (Figure 11c) (Vincent et al., 2015) and cracks and fissures(El-Maarry et al.,
448 2015). The steep sided pits and cliffs are thought to be correlated to the plumes of outgassing
449 (Vincent et al., 2016). Gassy outbursts were also noted to mobilise dust on asteroid Bennu, yet the
450 geomorphic effect if any in this setting remains unclear (Lauretta et al., 2019).

451 On other bodies, depressions are the most common landform associated with sublimation and can
452 be considered akin to karst on Earth. The perennial CO₂ ice found at the South Polar cap of Mars,
453 undergoes retreat each year in the form of enlarging and coalescing circular to elliptical steep sided
454 pits typically several hundred metres in diameter and metres deep, dubbed "swiss cheese" (Buhler et
455 al., 2017) (Figure 11d). The loss of excess water ice from the ground via sublimation in the mid-
456 latitudes of Mars results in "scalloped depressions" (Dundas et al., 2015; Soare et al., 2007) –
457 shallow-sloping depressions of hundreds of metres in extent, with an arcuate and steeper backwall.
458 In the some of the same regions, sublimation expands polygonally patterned contraction cracks
459 producing chains of pits and possibly cavities (Séjourné et al., 2011). Volatile loss has also been
460 invoked to explain shallow, steep-sided depressions on Mercury which are surrounded by a relatively
461 bright halo – "hollows" (Blewett et al., 2011) (Figure 11e). The discovery of these landforms was part
462 of the realisation that Mercury's crust is not actually depleted in volatiles as once thought (Nittler
463 and Weider, 2019).

464 The seasonal retreat of the CO₂ ice deposits across the surface of Mars results in a uniquely martian
465 process caused by basal sublimation of the CO₂ ice (Kieffer et al., 2006). CO₂ ice is translucent to solar
466 radiation, hence the increasing incoming solar radiation in late winter to early spring can heat the
467 regolith under the CO₂ ice, causing it to sublime and CO₂ gas to be trapped underneath it. The gas
468 pressure builds until the ice above breaks, releasing the gas in a jet which deposits dark dust from
469 under the ice onto the still bright icy surface. This phenomenon most commonly manifests itself as
470 dark fans or spots (Hansen et al., 2013) and on the steep slopes of dunes can even appear as digitate
471 (Gardin et al., 2010). The sediment mobilised under the ice is thought to explain the observation of
472 "spiders" – dendritic networks of channels leading to one or more "nodes" (Thomas et al., 2011)
473 (Figure 11f). Individual spiders can be hundreds of metres in size and they can extend across many
474 kilometres. Although spiders have not been observed to grow, similar branching networks have been
475 observed to appear and grow on dunes ("furrows") (Portyankina et al., 2010). Sediment mobilisation
476 by sublimating CO₂ is thought to explain ongoing sediment motions observed in martian gullies which
477 only occur in winter (Dundas et al., 2019). In particular, a uniquely martian morphology called "linear
478 gullies" is thought to be formed by levitating blocks of CO₂ ice falling from icy dune crests (Diniega et

479 al., 2013). Volatile loss is believed to drive the formation of gully-like-landforms on the asteroid Vesta
480 (Scully et al., 2015) and on Mercury (Malliband et al., 2019).

481 12 Discussion & Conclusions

482 Planetary geomorphology is distinctive from Earth-based geomorphology in that it is very reliant on
483 remote sensing and often a more global-scale perspective is taken on unravelling the formation of
484 landscapes and landforms. Satellite data of the Earth have spurred a number of studies taking a
485 similar planetary-scale perspective on Earth (Chen et al., 2019; Poulos et al., 2012), but more often
486 studies are local and/or regional in scale and scope. Planetary geomorphology is enticing to many,
487 because of the aspect of exploration and the possibility of making unusual discoveries on alien
488 worlds. Planetary geomorphology can drive key advances to better understand our own planet
489 (Baker, 1993; Sharp, 1980).

490 One of the major limitations of planetary geomorphology is the problem of equifinality and the
491 uncertainty of what landforms can be produced by processes unknown on Earth (Baker, 2014). To
492 infer processes from landforms and landscapes is not an exact science and always open to
493 interpretation. Access to the field can resolve many ambiguities on Earth, yet in a planetary context
494 this is rarely an option and can lead to impasses where researchers just do not have enough data to
495 disambiguate the leading hypotheses. Yet, as shown in this contribution, planetary geomorphology
496 remains an essential tool in understanding the internal and external forces shaping bodies in the
497 Solar System.

498 Planetary Geomorphology is likely to continue to grow, because the ability to interpret process from
499 remote sensing data is key to planning future missions, for example deciding where to land or
500 acquire certain types of data. Image and topographic data are the cornerstones of every new mission
501 and future exploration will only add to our database of new and surprising planetary landforms and
502 landscapes. Further, these landscapes have much to teach us about our own planet.

503 13 Acknowledgements

504 SJC is grateful to the CNES for financial support of her involvement in the ExoMars Trace Gas Orbiter
505 CaSSIS, MRO HiRISE and BepiColombo missions. SJC received funding from the regional government
506 Pays de la Loire scheme “Etoile Montantes” project METAFLows. The author thanks the spacecraft
507 and instrument engineering teams for the successful completion and operation of CaSSIS. CaSSIS is a
508 project of the University of Bern funded through the Swiss Space Office via ESA's PRODEX
509 programme. The instrument hardware development was also supported by the Italian Space Agency
510 (ASI) (ASI-INAF agreement no. I/018/12/0), INAF/ Astronomical Observatory of Padova, and the
511 Space Research Center (CBK) in Warsaw. Support from SGF (Budapest), the University of Arizona
512 (LPL) and NASA are also gratefully acknowledged. This study has been supported by the Italian Space
513 Agency (ASI-INAF agreement no. 2020-17-HH.0).

514 14 References

- 515
- 516 Ahrens, C.J., 2020. Modeling cryogenic mud volcanism on Pluto. *J. Volcanol. Geotherm. Res.* 406,
517 107070. <https://doi.org/10.1016/j.jvolgeores.2020.107070>
- 518 Ansan, V., Mangold, N., Masson, P., Gailhardis, E., Neukum, G., 2008. Topography of valley networks
519 on Mars from Mars Express High Resolution Stereo Camera digital elevation models. *J.
520 Geophys. Res.* 113, E07006. <https://doi.org/10.1029/2007JE002986>

- 521 Arvidson, R., Drozd, R.J., Hohenberg, C.M., Morgan, C.J., Poupeau, G., 1975. Horizontal transport of
522 the regolith, modification of features, and erosion rates on the lunar surface. *The moon* 13,
523 67–79. <https://doi.org/10.1007/BF00567508>
- 524 Baioni, D., Sgavetti, M., 2013. Karst terrains as possible lithologic and stratigraphic markers in
525 northern Sinus Meridiani, Mars. *Planet. Space Sci.* 75, 173–181.
<https://doi.org/10.1016/j.pss.2012.08.011>
- 527 Baker, V.R., 2014. Terrestrial analogs, planetary geology, and the nature of geological reasoning.
528 *Planet. Geol. Field Symp. Kitakyushu Jpn.* 2011 *Planet. Geol. Terr. Analogs* 95, 5–10.
<https://doi.org/10.1016/j.pss.2012.10.008>
- 530 Baker, V.R., 1993. Extraterrestrial geomorphology: science and philosophy of Earthlike planetary
531 landscapes, in: *Geomorphology: The Research Frontier and Beyond*. Elsevier, pp. 9–35.
<https://doi.org/10.1016/B978-0-444-89971-2.50006-7>
- 533 Baker, V.R., Kochel, R.C., 1979. Martian channel morphology: Maja and Kasei Valles. *J. Geophys. Res.*
534 84, 7961. <https://doi.org/10.1029/JB084iB14p07961>
- 535 Baker, V.R., Partridge, J.B., 1986. Small Martian valleys: Pristine and degraded morphology. *J.*
536 *Geophys. Res. Solid Earth* 91, 3561–3572. <https://doi.org/10.1029/JB091iB03p03561>
- 537 Baker, V.R., Strom, R.G., Gulick, V.C., Kargel, J.S., Komatsu, G., Kale, V.S., 1991. Ancient oceans, ice
538 sheets and the hydrological cycle on Mars. *Nature* 352, 589–594.
<https://doi.org/10.1038/352589a0>
- 540 Balme, M., Greeley, R., 2006. Dust devils on Earth and Mars. *Rev. Geophys.* 44, RG3003.
541 <https://doi.org/10.1029/2005RG000188>
- 542 Balme, M., Mangold, N., Baratoux, D., Costard, F., Gosselin, M., Masson, P., Pinet, P., Neukum, G.,
543 2006. Orientation and distribution of recent gullies in the southern hemisphere of Mars:
544 Observations from High Resolution Stereo Camera/Mars Express (HRSC/MEX) and Mars
545 Orbiter Camera/Mars Global Surveyor (MOC/MGS) data. *J. Geophys. Res. Planets* 111,
546 doi:10.1029/2005JE002607.
- 547 Balme, M.R., Pathare, A., Metzger, S.M., Towner, M.C., Lewis, S.R., Spiga, A., Fenton, L.K., Renno,
548 N.O., Elliott, H.M., Saca, F.A., Michaels, T.I., Russell, P., Verdasca, J., 2012. Field
549 measurements of horizontal forward motion velocities of terrestrial dust devils: Towards a
550 proxy for ambient winds on Mars and Earth. *Icarus* 221, 632–645.
<https://doi.org/10.1016/j.icarus.2012.08.021>
- 552 Basilevsky, A.T., Shalygin, E.V., Titov, D.V., Markiewicz, W.J., Scholten, F., Roatsch, Th., Kreslavsky,
553 M.A., Moroz, L.V., Ignatiev, N.I., Fiethe, B., Osterloh, B., Michalik, H., 2012. Geologic
554 interpretation of the near-infrared images of the surface taken by the Venus Monitoring
555 Camera, Venus Express. *Icarus* 217, 434–450. <https://doi.org/10.1016/j.icarus.2011.11.003>
- 556 Beddingfield, C.B., Beyer, R.A., Singer, K.N., McKinnon, W.B., Runyon, K., Grundy, W., Stern, S.A.,
557 Bray, V., Dhingra, R., Moore, J.M., Ennico, K., Olkin, C.B., Schenk, P., Spencer, J.R., Weaver,
558 H.A., Young, L.A., 2020. Landslides on Charon. *Icarus* 335, 113383.
<https://doi.org/10.1016/j.icarus.2019.07.017>
- 560 Bernhardt, H., Reiss, D., Hiesinger, H., Ivanov, M.A., 2016. The honeycomb terrain on the Hellas basin
561 floor, Mars: A case for salt or ice diapirism: Hellas' Honeycombs as Salt/Ice Diaps. *J.*
562 *Geophys. Res. Planets* 121, 714–738. <https://doi.org/10.1002/2016JE005007>
- 563 Bhardwaj, A., Sam, L., Martín-Torres, F.J., Zorzano, M.-P., Fonseca, R.M., 2017. Martian slope streaks
564 as plausible indicators of transient water activity. *Sci. Rep.* 7.
<https://doi.org/10.1038/s41598-017-07453-9>
- 566 Bickel, V.T., Aaron, J., Manconi, A., Loew, S., Mall, U., 2020. Impacts drive lunar rockfalls over billions
567 of years. *Nat. Commun.* 11, 2862. <https://doi.org/10.1038/s41467-020-16653-3>
- 568 Bickel, V.T., Kring, D.A., 2020. Lunar south pole boulders and boulder tracks: Implications for crew
569 and rover traverses. *Icarus* 348, 113850. <https://doi.org/10.1016/j.icarus.2020.113850>
- 570 Blewett, D.T., Chabot, N.L., Denevi, B.W., Ernst, C.M., Head, J.W., Izenberg, N.R., Murchie, S.L.,
571 Solomon, S.C., Nittler, L.R., McCoy, T.J., Xiao, Z., Baker, D.M.H., Fassett, C.I., Braden, S.E.,
572 Oberst, J., Scholten, F., Preusker, F., Hurwitz, D.M., 2011. Hollows on Mercury: MESSENGER

- 573 Evidence for Geologically Recent Volatile-Related Activity. *Science* 333, 1856–1859.
574 <https://doi.org/10.1126/science.1211681>
- 575 Bordiec, M., Carpy, S., Bourgeois, O., Herny, C., Massé, M., Perret, L., Claudin, P., Pochat, S., Douté,
576 S., 2020. Sublimation waves: Geomorphic markers of interactions between icy planetary
577 surfaces and winds. *Earth-Sci. Rev.* 211, 103350.
578 <https://doi.org/10.1016/j.earscirev.2020.103350>
- 579 Bourke, M.C., 2010. Barchan dune asymmetry: Observations from Mars and Earth. *Icarus* 205, 183–
580 197. <https://doi.org/10.1016/j.icarus.2009.08.023>
- 581 Bourke, M.C., Balme, M., Lewis, S., Lorenz, R.D., Parteli, E., 2019. Planetary Aeolian Geomorphology.
582 *Aeolian Geomorphol. New Introd.* 261–286.
- 583 Boyce, J.M., Mouginis-Mark, P., Robinson, M., 2020. The Tsiolkovskiy crater landslide, the moon: An
584 LROC view. *Icarus* 337, 113464. <https://doi.org/10.1016/j.icarus.2019.113464>
- 585 Bridges, N.T., Greeley, R., Haldemann, A.F.C., Herkenhoff, K.E., Kraft, M., Parker, T.J., Ward, A.W.,
586 1999. Ventifacts at the Pathfinder landing site. *J. Geophys. Res. Planets* 104, 8595–8615.
587 <https://doi.org/10.1029/98JE02550>
- 588 Brož, P., Hauber, E., 2012. A unique volcanic field in Tharsis, Mars: Pyroclastic cones as evidence for
589 explosive eruptions. *Icarus* 218, 88–99. <https://doi.org/10.1016/j.icarus.2011.11.030>
- 590 Brož, P., Krýza, O., Wilson, L., Conway, S.J., Hauber, E., Mazzini, A., Raack, J., Balme, M.R., Sylvest,
591 M.E., Patel, M.R., 2020. Experimental evidence for lava-like mud flows under Martian surface
592 conditions. *Nat. Geosci.* 13, 403–407. <https://doi.org/10.1038/s41561-020-0577-2>
- 593 Brunetti, M.T., Xiao, Z., Komatsu, G., Peruccacci, S., Guzzetti, F., 2015. Large rock slides in impact
594 craters on the Moon and Mercury. *Icarus* 260, 289–300.
595 <https://doi.org/10.1016/j.icarus.2015.07.014>
- 596 Brusnikin, E.S., Kreslavsky, M.A., Zubarev, A.E., Patratyi, V.D., Krasilnikov, S.S., Head, J.W.,
597 Karachevtseva, I.P., 2016. Topographic measurements of slope streaks on Mars. *Icarus* 278,
598 52–61. <https://doi.org/10.1016/j.icarus.2016.06.005>
- 599 Buhler, P.B., Ingersoll, A.P., Ehlmann, B.L., Fassett, C.I., Head, J.W., 2017. How the martian residual
600 south polar cap develops quasi-circular and heart-shaped pits, troughs, and moats. *Icarus*
601 286, 69–93. <https://doi.org/10.1016/j.icarus.2017.01.012>
- 602 Buldovicz, S.N., Khilimonyuk, V.Z., Bychkov, A.Y., Ospennikov, E.N., Vorobyev, S.A., Gunar, A.Y.,
603 Gorshkov, E.I., Chuvilin, E.M., Cherbunina, M.Y., Kotov, P.I., Lubnina, N.V., Motenko, R.G.,
604 Amanzhurov, R.M., 2018. Cryovolcanism on the Earth: Origin of a Spectacular Crater in the
605 Yamal Peninsula (Russia). *Sci. Rep.* 8, 13534. <https://doi.org/10.1038/s41598-018-31858-9>
- 606 Burns, J.A., 2010. The four hundred years of planetary science since Galileo and Kepler. *Nature* 466,
607 575–584. <https://doi.org/10.1038/nature09215>
- 608 Burr, D.M., Tanaka, K.L., Yoshikawa, K., 2009. Pingos on Earth and Mars. *Planet. Space Sci.* 57, 541–
609 555. <https://doi.org/10.1016/j.pss.2008.11.003>
- 610 Butcher, F.E.G., Balme, M.R., Conway, S.J., Gallagher, C.J., Arnold, N.S., Storrar, R.D., Lewis, S.R.,
611 Hagermann, A., 2020. Morphometry of a Glacier-Linked Esker in NW Tempe Terra, Mars, and
612 Implications for Sediment-Discharge Dynamics of Subglacial Drainage. *Earth Planet. Sci. Lett.*
613 542, 116325. <https://doi.org/10.1016/j.epsl.2020.116325>
- 614 Butcher, F.E.G., Conway, S.J., Arnold, N.S., 2016. Are the Dorsa Argentea on Mars eskers? *Icarus* 275,
615 65–84. <https://doi.org/10.1016/j.icarus.2016.03.028>
- 616 Byrne, P.K., Ghail, R.C., Şengör, A.M.C., James, P.B., Klimczak, C., Solomon, S.C., 2021. A globally
617 fragmented and mobile lithosphere on Venus. *Proc. Natl. Acad. Sci.* 118, e2025919118.
618 <https://doi.org/10.1073/pnas.2025919118>
- 619 Byrne, P.K., Klimczak, C., Celâl Şengör, A.M., Solomon, S.C., Watters, T.R., Hauck, II, S.A., 2014.
620 Mercury's global contraction much greater than earlier estimates. *Nat. Geosci.* 7, 301–307.
621 <https://doi.org/10.1038/ngeo2097>
- 622 Byrne, P.K., Klimczak, C., Williams, D.A., Hurwitz, D.M., Solomon, S.C., Head, J.W., Preusker, F.,
623 Oberst, J., 2013. An assemblage of lava flow features on Mercury: LAVA FLOW FEATURES ON
624 MERCURY. *J. Geophys. Res. Planets* 118, 1303–1322. <https://doi.org/10.1002/jgre.20052>

- 625 Cabrol, N., Grin, E.A., 1999. Distribution, Classification, and Ages of Martian Impact Crater Lakes.
626 *Icarus* 142, 160–172. <https://doi.org/10.1006/icar.1999.6191>
- 627 Carr, M., Head, J., 2019. Mars: Formation and fate of a frozen Hesperian ocean. *Icarus* 319, 433–443.
628 <https://doi.org/10.1016/j.icarus.2018.08.021>
- 629 Chen, S.-A., Michaelides, K., Grieve, S.W.D., Singer, M.B., 2019. Aridity is expressed in river
630 topography globally. *Nature* 573, 573–577. <https://doi.org/10.1038/s41586-019-1558-8>
- 631 Chuang, F.C., Beyer, R.A., McEwen, A.S., Thomson, B.J., 2007. HiRISE observations of slope streaks on
632 Mars. *Geophys. Res. Lett.* 34, doi:10.1029/2007GL031111. <https://doi.org/10.1029/2007GL031111>. Artn
633 I20204
- 634 Citron, R.I., Manga, M., Hemingway, D.J., 2018. Timing of oceans on Mars from shoreline
635 deformation. *Nature* 555, 643–646. <https://doi.org/10.1038/nature26144>
- 636 Collins, G.C., McKinnon, W.B., Moore, J.M., Nimmo, F., Pappalardo, R.T., Prockter, L.M., Schenk, P.M.,
637 2009. Tectonics of the outer planet satellites. *Planet. Tecton.* 11, 229.
- 638 Conway, S.J., Balme, M.R., 2016. A novel topographic parameterization scheme indicates that
639 martian gullies display the signature of liquid water. *Earth Planet. Sci. Lett.* 454, 36–45.
640 <https://doi.org/10.1016/j.epsl.2016.08.031>
- 641 Conway, S.J., de Haas, T., Harrison, T.N., 2019. Martian gullies: a comprehensive review of
642 observations, mechanisms and the insights from Earth analogues. *Geol. Soc. Lond. Spec.*
643 Publ. 467. <https://doi.org/10.1144/SP467.14>
- 644 Costard, F., Sejourne, A., Kargel, J., Godin, E., 2016. Modeling and observational occurrences of near-
645 surface drainage in Utopia Planitia, Mars. *Geomorphology* 275, 80–89.
646 <https://doi.org/10.1016/j.geomorph.2016.09.034>
- 647 Costard, F., Séjourné, A., Kelfoun, K., Clifford, S., Lavigne, F., Di Pietro, I., Bouley, S., 2017. Modeling
648 tsunami propagation and the emplacement of thumbprint terrain in an early Mars ocean:
649 TSUNAMIS ON MARS. *J. Geophys. Res. Planets* 122, 633–649.
650 <https://doi.org/10.1002/2016JE005230>
- 651 Crane, K., 2020. Structural interpretation of thrust fault-related landforms on Mercury using Earth
652 analogue fault models. *Geomorphology* 369, 107366.
653 <https://doi.org/10.1016/j.geomorph.2020.107366>
- 654 Crosta, G.B., Frattini, P., Valbuza, E., De Blasio, F.V., 2018. Introducing a New Inventory of Large
655 Martian Landslides. *Earth Space Sci.* 5, 89–119. <https://doi.org/10.1002/2017EA000324>
- 656 Davis, J.M., Balme, M., Grindrod, P.M., Williams, R.M.E., Gupta, S., 2016. Extensive Noachian fluvial
657 systems in Arabia Terra: Implications for early Martian climate. *Geology* 44, 847–850.
658 <https://doi.org/10.1130/G38247.1>
- 659 Day, M., Kocurek, G., 2016. Observations of an aeolian landscape: From surface to orbit in Gale
660 Crater. *Icarus* 280, 37–71. <https://doi.org/10.1016/j.icarus.2015.09.042>
- 661 de Haas, T., Hauber, E., Conway, S.J., van Steijn, H., Johnsson, A., Kleinhans, M.G., 2015. Earth-like
662 aqueous debris-flow activity on Mars at high orbital obliquity in the last million years. *Nat. Commun.* 6. <https://doi.org/10.1038/ncomms8543>
- 663 de Haas, T., Hauber, E., Kleinhans, M.G., 2013. Local late Amazonian boulder breakdown and
664 denudation rate on Mars. *Geophys. Res. Lett.* <https://doi.org/10.1002/grl.50726>
- 665 Dehouck, E., Mangold, N., Le Mouélic, S., Ansan, V., Poulet, F., 2010. Ismenius Cavus, Mars: A deep
666 paleolake with phyllosilicate deposits. *Planet. Space Sci.* 58, 941–946.
667 <https://doi.org/10.1016/j.pss.2010.02.005>
- 668 Denevi, B.W., Ernst, C.M., Meyer, H.M., Robinson, M.S., Murchie, S.L., Whitten, J.L., Head, J.W.,
669 Watters, T.R., Solomon, S.C., Ostrach, L.R., Chapman, C.R., Byrne, P.K., Klimczak, C.,
670 Peplowski, P.N., 2013. The distribution and origin of smooth plains on Mercury: SMOOTH
671 PLAINS ON MERCURY. *J. Geophys. Res. Planets* 118, 891–907.
672 <https://doi.org/10.1002/jgre.20075>
- 673 Di Achille, G., Hynek, B.M., 2010. Ancient ocean on Mars supported by global distribution of deltas
674 and valleys. *Nat. Geosci.* 3, 459–463. <https://doi.org/10.1038/ngeo891>

- 676 Diniega, S., Byrne, S., Bridges, N.T., Dundas, C.M., McEwen, A.S., 2010. Seasonality of present-day
677 Martian dune-gully activity. *Geology* 38, 1047–1050. <https://doi.org/10.1130/G31287.1>
- 678 Diniega, S., Hansen, C.J., McElwaine, J.N., Hugenholtz, C.H., Dundas, C.M., McEwen, A.S., Bourke,
679 M.C., 2013. A new dry hypothesis for the formation of martian linear gullies. *Icarus* 225, 526–
680 537. <https://doi.org/10.1016/j.icarus.2013.04.006>
- 681 Duarte, K.D., Schmidt, B.E., Chilton, H.T., Hughson, K.H.G., Sizemore, H.G., Ferrier, K.L., Buffo, J.J.,
682 Scully, J.E.C., Nathues, A., Platz, T., Landis, M., Byrne, S., Bland, M., Russell, C.T., Raymond,
683 C.A., 2019. Landslides on Ceres: Diversity and Geologic Context. *J. Geophys. Res. Planets*
684 2018JE005673. <https://doi.org/10.1029/2018JE005673>
- 685 Dundas, C.M., 2020. Geomorphological evidence for a dry dust avalanche origin of slope streaks on
686 Mars. *Nat. Geosci.* 13, 473–476. <https://doi.org/10.1038/s41561-020-0598-x>
- 687 Dundas, C.M., Byrne, S., McEwen, A.S., 2015. Modeling the development of martian sublimation
688 thermokarst landforms. *Icarus* 262, 154–169. <https://doi.org/10.1016/j.icarus.2015.07.033>
- 689 Dundas, C.M., McEwen, A.S., Diniega, S., Hansen, C.J., Byrne, S., McElwaine, J.N., 2019. The
690 Formation of Gullies on Mars Today. *Geol. Soc. Lond. Spec. Publ. Martian Gullies and their*
691 *Earth Analogues*. <https://doi.org/10.1144/SP467.5>
- 692 El Mir, C., Ramesh, K.T., Delbo, M., 2019. The efficiency of thermal fatigue in regolith generation on
693 small airless bodies. *Icarus* 333, 356–370. <https://doi.org/10.1016/j.icarus.2019.06.001>
- 694 El-Maarry, M.R., Thomas, N., Gracia-Berná, A., Marschall, R., Auger, A.-T., Groussin, O., Mottola, S.,
695 Pajola, M., Massironi, M., Marchi, S., Höfner, S., Preusker, F., Scholten, F., Jordá, L., Kührt, E.,
696 Keller, H.U., Sierks, H., A'Hearn, M.F., Barbieri, C., Barucci, M.A., Bertaux, J.-L., Bertini, I.,
697 Cremonese, G., Da Deppo, V., Davidsson, B., Debei, S., De Cecco, M., Deller, J., Güttler, C.,
698 Fornasier, S., Fulle, M., Gutierrez, P.J., Hofmann, M., Hviid, S.F., Ip, W.-H., Knollenberg, J.,
699 Koschny, D., Kovacs, G., Kramm, J.-R., Küppers, M., Lamy, P.L., Lara, L.M., Lazzarin, M., Lopez
700 Moreno, J.J., Marzari, F., Michalik, H., Naletto, G., Oklay, N., Pommerol, A., Rickman, H.,
701 Rodrigo, R., Tubiana, C., Vincent, J.-B., 2015. Fractures on comet 67P/Churyumov-
702 Gerasimenko observed by Rosetta/OSIRIS: FRACTURES ON COMET 67P. *Geophys. Res. Lett.*
703 42, 5170–5178. <https://doi.org/10.1002/2015GL064500>
- 704 Eppes, M.-C., Willis, A., Molaro, J., Abernathy, S., Zhou, B., 2015. Cracks in Martian boulders exhibit
705 preferred orientations that point to solar-induced thermal stress. *Nat. Commun.* 6, 6712.
706 <https://doi.org/10.1038/ncomms7712>
- 707 Ewing, R.C., Lapotre, M.G.A., Lewis, K.W., Day, M., Stein, N., Rubin, D.M., Sullivan, R., Banham, S.,
708 Lamb, M.P., Bridges, N.T., Gupta, S., Fischer, W.W., 2017. “Sedimentary processes of the
709 Bagnold Dunes: Implications for the eolian rock record of Mars”: Bagnold Dune Field
710 sedimentary processes. *J. Geophys. Res. Planets*. <https://doi.org/10.1002/2017JE005324>
- 711 Fassett, C.I., Crowley, M.C., Leight, C., Dyar, M.D., Minton, D.A., Hirabayashi, M., Thomson, B.J.,
712 Watters, W.A., 2017. Evidence for rapid topographic evolution and crater degradation on
713 Mercury from simple crater morphometry: Rapid Crater Degradation on Mercury. *Geophys.*
714 *Res. Lett.* <https://doi.org/10.1002/2017GL073769>
- 715 Fassett, C.I., Head III, J.W., 2008. The timing of martian valley network activity: Constraints from
716 buffered crater counting. *Icarus* 195, 61–89. <https://doi.org/10.1016/j.icarus.2007.12.009>
- 717 Fastook, J.L., Head, J.W., 2015. Glaciation in the Late Noachian Icy Highlands: Ice accumulation,
718 distribution, flow rates, basal melting, and top-down melting rates and patterns. *Planet.*
719 *Space Sci.* 106, 82–98. <https://doi.org/10.1016/j.pss.2014.11.028>
- 720 Feldman, W.C., Pathare, A., Maurice, S., Prettyman, T.H., Lawrence, D.J., Milliken, R.E., Travis, B.J.,
721 2011. Mars Odyssey neutron data: 2. Search for buried excess water ice deposits at nonpolar
722 latitudes on Mars. *J. Geophys. Res.* 116, E11009. <https://doi.org/10.1029/2011JE003806>
- 723 Ferri, F., Smith, P.H., Lemmon, M., Rennó, N.O., 2003. Dust devils as observed by Mars Pathfinder:
724 DUST DEVILS AS OBSERVED BY MARS PATHFINDER. *J. Geophys. Res. Planets* 108.
725 <https://doi.org/10.1029/2000JE001421>

- 726 Ferrill, D.A., Wyrick, D.Y., Smart, K.J., 2011. Coseismic, dilational-fault and extension-fracture related
727 pit chain formation in Iceland: Analog for pit chains on Mars. *Lithosphere* 3, 133–142.
728 <https://doi.org/10.1130/L123.1>
- 729 Gallagher, C., Balme, M., 2015. Eskers in a complete, wet-based glacial system in the Phlegra Montes
730 region, Mars. *Earth Planet. Sci. Lett.* 431, 96–109. <https://doi.org/10.1016/j.epsl.2015.09.023>
- 731 Gallagher, C., Balme, M.R., Conway, S.J., Grindrod, P.M., 2011. Sorted clastic stripes, lobes and
732 associated gullies in high-latitude craters on Mars: Landforms indicative of very recent,
733 polycyclic ground-ice thaw and liquid flows. *Icarus* 211, 458–471.
734 <https://doi.org/10.1016/j.icarus.2010.09.010>
- 735 Gardin, E., Allemand, P., Quantin, C., Thollot, P., 2010. Defrosting, dark flow features, and dune
736 activity on Mars: Example in Russell crater. *J Geophys Res* 115, doi:10.1029/2009JE003515.
737 <https://doi.org/10.1029/2009je003515>
- 738 Gastineau, R., Conway, S.J., Johnsson, A., Eichel, J., Mangold, N., Grindrod, P.M., Izquierdo, T., 2020.
739 Small-scale lobate hillslope features on Mars: A comparative 3D morphological study with
740 terrestrial solifluction lobes and zebra stripe lobes. *Icarus* accepted.
- 741 Ghatan, G., Zimbelman, J., 2006. Paucity of candidate coastal constructional landforms along
742 proposed shorelines on Mars: Implications for a northern lowlands-filling ocean. *Icarus* 185,
743 171–196. <https://doi.org/10.1016/j.icarus.2006.06.007>
- 744 Goudge, T.A., Aureli, K.L., Head, J.W., Fassett, C.I., Mustard, J.F., 2015. Classification and analysis of
745 candidate impact crater-hosted closed-basin lakes on Mars. *Icarus* 260, 346–367.
746 <https://doi.org/10.1016/j.icarus.2015.07.026>
- 747 Goudge, T.A., Fassett, C.I., Head, J.W., Mustard, J.F., Aureli, K.L., 2016. Insights into surface runoff on
748 early Mars from paleolake basin morphology and stratigraphy. *Geology* 44, 419–422.
749 <https://doi.org/10.1130/G37734.1>
- 750 Goudie, A.S., 2007. Mega-Yardangs: A Global Analysis: Mega-yardangs: A global analysis. *Geogr.*
751 *Compass* 1, 65–81. <https://doi.org/10.1111/j.1749-8198.2006.00003.x>
- 752 Grau Galofre, A., Jellinek, A.M., Osinski, G.R., 2020. Valley formation on early Mars by subglacial and
753 fluvial erosion. *Nat. Geosci.* <https://doi.org/10.1038/s41561-020-0618-x>
- 754 Greeley, R., Arvidson, R.E., Barlett, P.W., Blaney, D., Cabrol, N.A., Christensen, P.R., Fergason, R.L.,
755 Golombek, M.P., Landis, G.A., Lemmon, M.T., McLennan, S.M., Maki, J.N., Michaels, T.,
756 Moersch, J.E., Neakrase, L.D.V., Rafkin, S.C.R., Richter, L., Squyres, S.W., de Souza, P.A.,
757 Sullivan, R.J., Thompson, S.D., Whelley, P.L., 2006a. Gusev crater: Wind-related features and
758 processes observed by the Mars Exploration Rover Spirit: GUSEV CRATER OBSERVED BY
759 SPIRIT. *J. Geophys. Res. Planets* 111, n/a-n/a. <https://doi.org/10.1029/2005JE002491>
- 760 Greeley, R., Bender, K., Thomas, P.E., Schubert, G., Limonadi, D., Weitz, C.M., 1995. Wind-Related
761 Features and Processes on Venus: Summary of Magellan Results. *Icarus* 115, 399–420.
762 <https://doi.org/10.1006/icar.1995.1107>
- 763 Greeley, R., Whelley, P.L., Arvidson, R.E., Cabrol, N.A., Foley, D.J., Franklin, B.J., Geissler, P.G.,
764 Golombek, M.P., Kuzmin, R.O., Landis, G.A., Lemmon, M.T., Neakrase, L.D.V., Squyres, S.W.,
765 Thompson, S.D., 2006b. Active dust devils in Gusev crater, Mars: Observations from the Mars
766 Exploration Rover Spirit: ACTIVE DUST DEVILS IN GUSEV CRATER, MARS. *J. Geophys. Res.*
767 *Planets* 111, n/a-n/a. <https://doi.org/10.1029/2006JE002743>
- 768 Grindrod, P.M., Balme, M.R., 2010. Groundwater processes in Hebes Chasma, Mars: GROUNDWATER
769 AND HYDRATES ON MARS. *Geophys. Res. Lett.* 37, n/a-n/a.
770 <https://doi.org/10.1029/2010GL044122>
- 771 Grindrod, P.M., Davis, J.M., Conway, S.J., de Haas, T., 2021. Active Boulder Falls in Terra Sirenum,
772 Mars: Constraints on Timing and Causes. *Geophys. Res. Lett.* Accepted.
- 773 Gustafson, J.O., Bell, J.F., Gaddis, L.R., Hawke, B.R., Giguere, T.A., 2012. Characterization of previously
774 unidentified lunar pyroclastic deposits using Lunar Reconnaissance Orbiter Camera data:
775 NEW PYROCLASTIC DEPOSITS. *J. Geophys. Res. Planets* 117, n/a-n/a.
776 <https://doi.org/10.1029/2011JE003893>

- 777 Hansen, C.J., Byrne, S., Portyankina, G., Bourke, M., Dundas, C., McEwen, A., Mellon, M., Pommerol,
778 A., Thomas, N., 2013. Observations of the northern seasonal polar cap on Mars: I. Spring
779 sublimation activity and processes. *Mars Polar Sci.* V 225, 881–897.
780 <https://doi.org/10.1016/j.icarus.2012.09.024>
- 781 Hargitai, H., Kereszturi, Á. (Eds.), 2015. *Encyclopedia of Planetary Landforms*, Springer reference.
782 Springer, New York.
- 783 Harrison, K.P., Grimm, R.E., 2003. Rheological constraints on martian landslides. *Icarus* 163, 347–362.
784 [https://doi.org/10.1016/S0019-1035\(03\)00045-9](https://doi.org/10.1016/S0019-1035(03)00045-9)
- 785 Harrison, T.N., Osinski, G.R., Tornabene, L.L., Jones, E., 2015. Global Documentation of Gullies with
786 the Mars Reconnaissance Orbiter Context Camera and Implications for Their Formation.
787 *Icarus* 252, 236–254. <https://doi.org/10.1016/j.icarus.2015.01.022>
- 788 Hartmann, W.K., Neukum, G., 2001. Cratering Chronology and the Evolution of Mars. *Space Sci. Rev.*
789 96, 165–194. <https://doi.org/10.1023/A:1011945222010>
- 790 Head, J.W., Crumpler, L.S., Aubele, J.C., Guest, J.E., Saunders, R.S., 1992. Venus volcanism:
791 Classification of volcanic features and structures, associations, and global distribution from
792 Magellan data. *J. Geophys. Res.* 97, 13153. <https://doi.org/10.1029/92JE01273>
- 793 Head, J.W., Kreslavsky, M.A., Marchant, D.R., 2011. Pitted rock surfaces on Mars: A mechanism of
794 formation by transient melting of snow and ice. *J. Geophys. Res.* 116, E09007.
795 <https://doi.org/10.1029/2011JE003826>
- 796 Head, J.W., Marchant, D.R., 2003. Cold-based mountain glaciers on Mars: Western Arsia Mons.
797 *Geology* 31, 641–644. [https://doi.org/10.1130/0091-7613\(2003\)031<0641:CMGOMW>2.0.CO;2](https://doi.org/10.1130/0091-7613(2003)031<0641:CMGOMW>2.0.CO;2)
- 799 Herrero-Gil, A., Egea-González, I., Ruiz, J., Romeo, I., 2019. Structural modeling of lobate scarps in the
800 NW margin of Argyre impact basin, Mars. *Icarus* 319, 367–380.
801 <https://doi.org/10.1016/j.icarus.2018.09.027>
- 802 Hiesinger, H., Marchi, S., Schmedemann, N., Schenk, P., Pasckert, J.H., Neesemann, A., O'Brien, D.P.,
803 Kneissl, T., Ermakov, A.I., Fu, R.R., Bland, M.T., Nathues, A., Platz, T., Williams, D.A., Jaumann,
804 R., Castillo-Rogez, J.C., Ruesch, O., Schmidt, B., Park, R.S., Preusker, F., Buczkowski, D.L.,
805 Russell, C.T., Raymond, C.A., 2016. Cratering on Ceres: Implications for its crust and
806 evolution. *Science* 353, aaf4759. <https://doi.org/10.1126/science.aaf4759>
- 807 Hirata, N., Miyamoto, H., Showman, A.P., 2014. Particle deposition on the saturnian satellites from
808 ephemeral cryovolcanism on Enceladus. *Geophys. Res. Lett.* 41, 4135–4141.
809 <https://doi.org/10.1002/2014GL060470>
- 810 Hötz, F., Cintala, M.J., Rochelle, W.C., Kirk, B., 1999. Collisionally Processed Rocks on Mars. *Science*
811 285, 2105–2107. <https://doi.org/10.1126/science.285.5436.2105>
- 812 Howard, A.D., Moore, J.M., Umurhan, O.M., White, O.L., Anderson, R.S., McKinnon, W.B., Spencer,
813 J.R., Schenk, P.M., Beyer, R.A., Stern, S.A., Ennico, K., Olkin, C.B., Weaver, H.A., Young, L.A.,
814 2017a. Present and past glaciation on Pluto. *Spec. Issue Pluto Syst.* 287, 287–300.
815 <https://doi.org/10.1016/j.icarus.2016.07.006>
- 816 Howard, A.D., Moore, J.M., White, O.L., Umurhan, O.M., Schenk, P.M., Grundy, W.M., Schmitt, B.,
817 Philippe, S., McKinnon, W.B., Spencer, J.R., Beyer, R.A., Stern, S.A., Ennico, K., Olkin, C.B.,
818 Weaver, H.A., Young, L.A., 2017b. Pluto: Pits and mantles on uplands north and east of
819 Sputnik Planitia. *Icarus* 293, 218–230. <https://doi.org/10.1016/j.icarus.2017.02.027>
- 820 Hurwitz, D.M., Head, J.W., Hiesinger, H., 2013. Lunar sinuous rilles: Distribution, characteristics, and
821 implications for their origin. *Planet. Space Sci.* 79–80, 1–38.
822 <https://doi.org/10.1016/j.pss.2012.10.019>
- 823 Ielpi, A., Lapôtre, M.G.A., 2020. A tenfold slowdown in river meander migration driven by plant life.
824 *Nat. Geosci.* 13, 82–86. <https://doi.org/10.1038/s41561-019-0491-7>
- 825 Jia, P., Andreotti, B., Claudin, P., 2017. Giant ripples on comet 67P/Churyumov–Gerasimenko
826 sculpted by sunset thermal wind. *Proc. Natl. Acad. Sci.* 114, 2509–2514.
827 <https://doi.org/10.1073/pnas.1612176114>

- 828 Johnson, B.C., Campbell, C.S., 2017. Drop Height and Volume Control the Mobility of Long-Runout
829 Landslides on the Earth and Mars: The Mobility of Long-Runout Landslides on the Earth and
830 Mars. *Geophys. Res. Lett.* <https://doi.org/10.1002/2017GL076113>
- 831 Johnson, B.C., Sori, M.M., 2020. Landslide Morphology and Mobility on Ceres Controlled by
832 Topography. *J. Geophys. Res. Planets* 125. <https://doi.org/10.1029/2020JE006640>
- 833 Johnsson, A., Reiss, D., Hauber, E., Zanetti, M., Hiesinger, H., Johansson, L., Olvmo, M., 2012.
834 Periglacial mass-wasting landforms on Mars suggestive of transient liquid water in the recent
835 past: Insights from solifluction lobes on Svalbard. *Icarus* 218, 489–505.
836 <https://doi.org/10.1016/j.icarus.2011.12.021>
- 837 Jones, A.P., Pickering, K.T., 2003. Evidence for aqueous fluid–sediment transport and erosional
838 processes on Venus. *J. Geol. Soc.* 160, 319–327. <https://doi.org/10.1144/0016-764902-111>
- 839 Kargel, J.S., 1995. Cryovolcanism on the Icy Satellites, in: Chahine, M.T., A’Hearn, M.F., Rahe, J.,
840 Solomon, P., Nickle, N.L. (Eds.), *Comparative Planetology with an Earth Perspective*. Springer
841 Netherlands, Dordrecht, pp. 101–113. https://doi.org/10.1007/978-94-017-1092-3_12
- 842 Kargel, J.S., Kirk, R.L., Fegley, B., Treiman, A.H., 1994. Carbonate-Sulfate Volcanism on Venus? *Icarus*
843 112, 219–252. <https://doi.org/10.1006/icar.1994.1179>
- 844 Karlsson, N.B., Schmidt, L.S., Hvidberg, C.S., 2015. Volume of Martian midlatitude glaciers from radar
845 observations and ice flow modeling. *Geophys. Res. Lett.* 42, 2627–2633.
846 <https://doi.org/10.1002/2015GL063219>
- 847 Kattenhorn, S.A., Prockter, L.M., 2014. Evidence for subduction in the ice shell of Europa. *Nat. Geosci.*
848 7, 762–767. <https://doi.org/10.1038/ngeo2245>
- 849 Kenkemann, T., Poelchau, M.H., Wulf, G., 2014. Structural geology of impact craters. *J. Struct. Geol.*
850 62, 156–182. <https://doi.org/10.1016/j.jsg.2014.01.015>
- 851 Kerber, L., Head, J.W., Blewett, D.T., Solomon, S.C., Wilson, L., Murchie, S.L., Robinson, M.S., Denevi,
852 B.W., Domingue, D.L., 2011. The global distribution of pyroclastic deposits on Mercury: The
853 view from MESSENGER flybys 1–3. *Planet. Space Sci.* 59, 1895–1909.
854 <https://doi.org/10.1016/j.pss.2011.03.020>
- 855 Kieffer, H.H., 1990. H₂O grain size and the amount of dust in Mars' residual north polar CAP. *J.*
856 *Geophys. Res.* 95, 1481–1493.
- 857 Kieffer, H.H., Christensen, P.R., Titus, T.N., 2006. CO₂ jets formed by sublimation beneath translucent
858 slab ice in Mars' seasonal south polar ice cap. *Nature* 442, 793–796.
859 <https://doi.org/10.1038/nature04945>
- 860 Knight, J., 2008. The environmental significance of ventifacts: A critical review. *Earth-Sci. Rev.* 86, 89–
861 105. <https://doi.org/10.1016/j.earscirev.2007.08.003>
- 862 Kok, J.F., Parteli, E.J.R., Michaels, T.I., Karam, D.B., 2012. The physics of wind-blown sand and dust.
863 *Rep. Prog. Phys.* 75, 106901. <https://doi.org/10.1088/0034-4885/75/10/106901>
- 864 Komatsu, G., Baker, V.R., 1994. Meander properties of Venusian channels. *Geology* 22, 67.
865 [https://doi.org/10.1130/0091-7613\(1994\)022<0067:MPOVC>2.3.CO;2](https://doi.org/10.1130/0091-7613(1994)022<0067:MPOVC>2.3.CO;2)
- 866 Laity, J.E., Bridges, N.T., 2009. Ventifacts on Earth and Mars: Analytical, field, and laboratory studies
867 supporting sand abrasion and windward feature development. *Geomorphology* 105, 202–
868 217. <https://doi.org/10.1016/j.geomorph.2008.09.014>
- 869 Lapotre, M.G.A., Lamb, M.P., 2018. Substrate controls on valley formation by groundwater on Earth
870 and Mars. *Geology* 46, 531–534. <https://doi.org/10.1130/G40007.1>
- 871 Lapôtre, M.G.A., O’Rourke, J.G., Schaefer, L.K., Siebach, K.L., Spalding, C., Tikoo, S.M., Wordsworth,
872 R.D., 2020. Probing space to understand Earth. *Nat. Rev. Earth Environ.* 1, 170–181.
873 <https://doi.org/10.1038/s43017-020-0029-y>
- 874 Lauretta, D.S., Hergenrother, C.W., Chesley, S.R., Leonard, J.M., Pelgrift, J.Y., Adam, C.D., Al Asad, M.,
875 Antreasian, P.G., Ballouz, R.-L., Becker, K.J., Bennett, C.A., Bos, B.J., Bottke, W.F., Brozović,
876 M., Campins, H., Connolly, H.C., Daly, M.G., Davis, A.B., de León, J., DellaGiustina, D.N.,
877 Drouet d’Aubigny, C.Y., Dworkin, J.P., Emery, J.P., Farnocchia, D., Glavin, D.P., Golish, D.R.,
878 Hartzell, C.M., Jacobson, R.A., Jawin, E.R., Jenniskens, P., Kidd, J.N., Lessac-Chenen, E.J., Li, J.-
879 Y., Libourel, G., Licandro, J., Liounis, A.J., Maleszewski, C.K., Manzoni, C., May, B., McCarthy,

- 880 L.K., McMahon, J.W., Michel, P., Molaro, J.L., Moreau, M.C., Nelson, D.S., Owen, W.M., Rizk,
881 B., Roper, H.L., Rozitis, B., Sahr, E.M., Scheeres, D.J., Seabrook, J.A., Selznick, S.H., Takahashi,
882 Y., Thuillet, F., Tricarico, P., Vokrouhlický, D., Wolner, C.W.V., 2019. Episodes of particle
883 ejection from the surface of the active asteroid (101955) Bennu. *Science* 366, eaay3544.
884 <https://doi.org/10.1126/science.aay3544>
- 885 Leverington, D.W., 2011. A volcanic origin for the outflow channels of Mars: Key evidence and major
886 implications. *Geomorphology* 132, 51–75. <https://doi.org/10.1016/j.geomorph.2011.05.022>
- 887 Levin, J.N., Dickson, J.L., Lamb, M.P., 2021. Evaluating the Role of Volatiles in Bedrock Chute
888 Formation on the Moon and Mars. *Icarus* In review.
- 889 Lorenz, R., Zimbelman, J.R., 2014. Dune worlds: how windblown sand shapes planetary landscapes,
890 Springer Praxis books. Geophysical sciences. Springer ; Published in association with Praxis
891 Publishing, Berlin ; New York ; London : Chichester, UK.
- 892 Lucchetti, A., Penasa, L., Pajola, M., Massironi, M., Brunetti, M.T., Cremonese, G., Oklay, N., Vincent,
893 J., Mottola, S., Fornasier, S., Sierks, H., Nalletto, G., Lamy, P.L., Rodrigo, R., Koschny, D.,
894 Davidsson, B., Barbieri, C., Barucci, M.A., Bertaux, J., Bertini, I., Bodewits, D., Cambianica, P.,
895 Da Deppo, V., Debei, S., De Cecco, M., Deller, J., Ferrari, S., Ferri, F., Franceschi, M., Fulle, M.,
896 Gutiérrez, P., Güttler, C., Ip, W., Keller, U., Lara, L., Lazzarin, M., Moreno, J.L., Marzari, F.,
897 Tubiana, C., 2019. The Rocky-Like Behavior of Cometary Landslides on 67P/Churyumov-
898 Gerasimenko. *Geophys. Res. Lett.* 46, 14336–14346. <https://doi.org/10.1029/2019GL085132>
- 899 Luo, W., Howard, A.D., 2008. Computer simulation of the role of groundwater seepage in forming
900 Martian valley networks. *J. Geophys. Res. Planets* 113, E05002.
901 <https://doi.org/10.1029/2007JE002981>
- 902 MacKenzie, S.M., Barnes, J.W., Sotin, C., Soderblom, J.M., Le Mouélic, S., Rodriguez, S., Baines, K.H.,
903 Buratti, B.J., Clark, R.N., Nicholson, P.D., McCord, T.B., 2014. Evidence of Titan's climate
904 history from evaporite distribution. *Icarus* 243, 191–207.
905 <https://doi.org/10.1016/j.icarus.2014.08.022>
- 906 Madeleine, J.-B., Forget, F., Millour, E., Montabone, L., Wolff, M.J., 2011. Revisiting the radiative
907 impact of dust on Mars using the LMD Global Climate Model. *J. Geophys. Res.* 116, E11010.
908 <https://doi.org/10.1029/2011JE003855>
- 909 Malin, M.C., Edgett, K.S., 2000. Evidence for recent groundwater seepage and surface runoff on
910 Mars. *Science* 288, 2330–2335. <https://doi.org/10.1126/science.288.5475.2330>
- 911 Malin, M.C., Edgett, K.S., 1999. Oceans or seas in the Martian northern lowlands: High resolution
912 imaging tests of proposed coastlines. *Geophys. Res. Lett.* 26, 3049–3052.
913 <https://doi.org/10.1029/1999GL002342>
- 914 Malliband, C.C., Conway, S.J., Rothery, D.A., Balme, M.R., 2019. Potential Identification of Downslope
915 Mass Movements on Mercury Driven by Volatile-Loss, in: Lunar and Planetary Science
916 Conference. p. #1804.
- 917 Mangold, N., 2012. Fluvial landforms on fresh impact ejecta on Mars. *Planet. Space Sci.* 62, 69–85.
918 <https://doi.org/10.1016/j.pss.2011.12.009>
- 919 Mangold, N., 2011. Ice sublimation as a geomorphic process: A planetary perspective.
920 *Geomorphology* 126, 1–17. <https://doi.org/10.1016/j.geomorph.2010.11.009>
- 921 Mangold, N., 2005. High latitude patterned grounds on Mars: Classification, distribution and climatic
922 control. *Mars Polar Sci. III* 174, 336–359. <https://doi.org/10.1016/j.icarus.2004.07.030>
- 923 Mangold, N., Kite, E.S., Kleinhans, M.G., Newsom, H., Ansan, V., Hauber, E., Kraal, E., Quantin, C.,
924 Tanaka, K., 2012. The origin and timing of fluvial activity at Eberswalde crater, Mars. *Icarus*
925 220, 530–551. <https://doi.org/10.1016/j.icarus.2012.05.026>
- 926 Marra, W.A., McLellan, S.J., Parsons, D.R., Murphy, B.J., Hauber, E., Kleinhans, M.G., 2015.
927 Groundwater seepage landscapes from distant and local sources in experiments and on
928 Mars. *Earth Surf Dynam* 3, 389–408. <https://doi.org/10.5194/esurf-3-389-2015>
- 929 Mastrogiovanni, M., Poggiali, V., Hayes, A.G., Lunine, J.I., Seu, R., Mitri, G., Lorenz, R.D., 2019. Deep
930 and methane-rich lakes on Titan. *Nat. Astron.* 3, 535–542. <https://doi.org/10.1038/s41550-019-0714-2>

- 932 Masursky, H., 1973. An overview of geological results from Mariner 9. *J. Geophys. Res.* 78, 4009–
933 4030. <https://doi.org/10.1029/JB078i020p04009>
- 934 McEwen, A.S., 1998. High-Temperature Silicate Volcanism on Jupiter's Moon Io. *Science* 281, 87–90.
935 <https://doi.org/10.1126/science.281.5373.87>
- 936 McEwen, A.S., 1989. Mobility of large rock avalanches: Evidence from Valles Marineris, Mars.
937 *Geology* 17, 1111–1114. [https://doi.org/10.1130/0091-7613\(1989\)017<1111:MOLRAE>2.3.CO;2](https://doi.org/10.1130/0091-7613(1989)017<1111:MOLRAE>2.3.CO;2)
- 938 McEwen, A.S., Ojha, L., Dundas, C.M., Mattson, S.S., Byrne, S., Wray, J.J., Cull, S.C., Murchie, S.L.,
939 Thomas, N., Gulick, V.C., 2011. Seasonal Flows on Warm Martian Slopes. *Science* 333, 740–
940 743. <https://doi.org/10.1126/science.1204816>
- 941 Mellon, M.T., Arvidson, R.E., Sizemore, H.G., Searls, M.L., Blaney, D.L., Cull, S., Hecht, M.H., Heet, T.L.,
942 Keller, H.U., Lemmon, M.T., Markiewicz, W.J., Ming, D.W., Morris, R.V., Pike, W.T., Zent, A.P.,
943 2009. Ground ice at the Phoenix Landing Site: Stability state and origin. *J. Geophys. Res. Planets* 114, E00E07. <https://doi.org/10.1029/2009JE003417>
- 944 Melosh, H.J., 1989. Impact cratering: a geologic process, Oxford monographs on geology and
945 geophysics ; no. 11. Oxford University Press.
- 946 Michael, G.G., Neukum, G., 2010. Planetary surface dating from crater size–frequency distribution
947 measurements: Partial resurfacing events and statistical age uncertainty. *Earth Planet. Sci. Lett.* 294, 223–229. <https://doi.org/10.1016/j.epsl.2009.12.041>
- 948 Miyamoto, H., 2004. Fluid dynamical implications of anastomosing slope streaks on Mars. *J. Geophys. Res.* 109. <https://doi.org/10.1029/2003JE002234>
- 949 Molaro, J., Byrne, S., 2012. Rates of temperature change of airless landscapes and implications for
950 thermal stress weathering. *J Geophys Res* 117, E10011.
951 <https://doi.org/10.1029/2012JE004138>
- 952 Moore, J.M., Asphaug, E., Morrison, D., Spencer, J.R., Chapman, C.R., Bierhaus, B., Sullivan, R.J.,
953 Chuang, F.C., Klemaszewski, J.E., Greeley, R., Bender, K.C., Geissler, P.E., Helfenstein, P.,
954 Pilcher, C.B., 1999. Mass Movement and Landform Degradation on the Icy Galilean Satellites:
955 Results of the Galileo Nominal Mission. *Icarus* 140, 294–312.
956 <https://doi.org/10.1006/icar.1999.6132>
- 957 Moore, J.M., Howard, A.D., 2010. Are the basins of Titan's Hotei Regio and Tui Regio sites of former
958 low latitude seas?: FORMER LOW LATITUDE SEAS OF TITAN. *Geophys. Res. Lett.* 37, n/a-n/a.
959 <https://doi.org/10.1029/2010GL045234>
- 960 Moore, J.M., Howard, A.D., Umurhan, O.M., White, O.L., Schenk, P.M., Beyer, R.A., McKinnon, W.B.,
961 Spencer, J.R., Singer, K.N., Grundy, W.M., Earle, A.M., Schmitt, B., Protopapa, S., Nimmo, F.,
962 Cruikshank, D.P., Hinson, D.P., Young, L.A., Stern, S.A., Weaver, H.A., Olkin, C.B., Ennico, K.,
963 Collins, G., Bertrand, T., Forget, F., Scipioni, F., 2018. Bladed Terrain on Pluto: Possible origins
964 and evolution. *Icarus* 300, 129–144. <https://doi.org/10.1016/j.icarus.2017.08.031>
- 965 Morris, E.C., 1982. Aureole deposits of the Martian volcano Olympus Mons. *J. Geophys. Res.* 87,
966 1164–1178.
- 967 Mottola, S., Arnold, G., Grothues, H.-G., Jaumann, R., Michaelis, H., Neukum, G., Bibring, J.-P.,
968 Schroder, S.E., Hamm, M., Otto, K.A., Pelivan, I., Proffe, G., Scholten, F., Tirsch, D., Kreslavsky, M.,
969 Remetean, E., Souvannavong, F., Dolives, B., 2015. The structure of the regolith on
970 67P/Churyumov-Gerasimenko from ROLIS descent imaging. *Science* 349, aab0232–aab0232.
971 <https://doi.org/10.1126/science.aab0232>
- 972 Mustard, J.F., Cooper, C.D., Rifkin, M.K., 2001. Evidence for recent climate change on Mars from the
973 identification of youthful near-surface ground ice. *Nature* 412, 411–414.
974 <https://doi.org/10.1038/35086515>
- 975 Nahm, A.L., Schultz, R.A., 2011. Magnitude of global contraction on Mars from analysis of surface
976 faults: Implications for martian thermal history. *Icarus* 211, 389–400.
977 <https://doi.org/10.1016/j.icarus.2010.11.003>
- 978 Nathues, A., Schmedemann, N., Thangjam, G., Pasckert, J.H., Mengel, K., Castillo-Rogez, J., Cloutis,
979 E.A., Hiesinger, H., Hoffmann, M., Le Corre, L., Li, J.-Y., Pieters, C., Raymond, C.A., Reddy, V.,

- 984 Ruesch, O., Williams, D.A., 2020. Recent cryovolcanic activity at Occator crater on Ceres. *Nat.*
985 *Astron.* 4, 794–801. <https://doi.org/10.1038/s41550-020-1146-8>
- 986 Nittler, L.R., Weider, S.Z., 2019. The Surface Composition of Mercury. *Elements* 15, 33–38.
987 <https://doi.org/10.2138/gselements.15.1.33>
- 988 Obleitner, F., Spötl, C., 2011. The mass and energy balance of ice within the Eisriesenwelt cave,
989 Austria. *The Cryosphere* 5, 245–257. <https://doi.org/10.5194/tc-5-245-2011>
- 990 Oehler, D.Z., Allen, C.C., 2010. Evidence for pervasive mud volcanism in Acidalia Planitia, Mars. *Icarus*
991 208, 636–657. <https://doi.org/10.1016/j.icarus.2010.03.031>
- 992 Ojha, L., McEwen, A., Dundas, C., Byrne, S., Mattson, S., Wray, J., Masse, M., Schaefer, E., 2014.
993 HiRISE observations of Recurring Slope Lineae (RSL) during southern summer on Mars. *Icarus*
994 231, 365–376. <https://doi.org/10.1016/j.icarus.2013.12.021>
- 995 Osinski, G.R., Tornabene, L.L., Banerjee, N.R., Cockell, C.S., Flemming, R., Izawa, M.R.M.,
996 McCutcheon, J., Parnell, J., Preston, L.J., Pickersgill, A.E., Pontefract, A., Sapers, H.M.,
997 Southam, G., 2013. Impact-generated hydrothermal systems on Earth and Mars. *Icarus* 224,
998 347–363. <https://doi.org/10.1016/j.icarus.2012.08.030>
- 999 Paillou, P., Seignovert, B., Radebaugh, J., Wall, S., 2016. Radar scattering of linear dunes and mega-
1000 yardangs: Application to Titan. *Icarus* 270, 211–221.
1001 <https://doi.org/10.1016/j.icarus.2015.07.038>
- 1002 Parker, T.J., Gorsline, D.S., Saunders, R.S., Pieri, D.C., Schneeberger, D.M., 1993. Coastal
1003 geomorphology of the Martian northern plains. *J. Geophys. Res.* 98, 11061.
1004 <https://doi.org/10.1029/93JE00618>
- 1005 Parsons, R.A., Nimmo, F., Miyamoto, H., 2011. Constraints on martian lobate debris apron evolution
1006 and rheology from numerical modeling of ice flow. *Icarus* 214, 246–257.
1007 <https://doi.org/10.1016/j.icarus.2011.04.014>
- 1008 Peale, S.J., Schubert, G., Lingenfelter, R.E., 1968. Distribution of Sinuous Rilles and Water on the
1009 Moon. *Nature* 220, 1222–1225. <https://doi.org/10.1038/2201222a0>
- 1010 Perron, J.T., Lamb, M.P., Koven, C.D., Fung, I.Y., Yager, E., Ádámkovics, M., 2006. Valley formation
1011 and methane precipitation rates on Titan. *J. Geophys. Res.* 111, E11001.
1012 <https://doi.org/10.1029/2005JE002602>
- 1013 Petersen, E.I., Holt, J.W., Levy, J.S., 2018. High Ice Purity of Martian Lobate Debris Aprons at the
1014 Regional Scale: Evidence From an Orbital Radar Sounding Survey in Deuteronilus and
1015 Protonilus Mensae. *Geophys. Res. Lett.* 45, 11,595–11,604.
1016 <https://doi.org/10.1029/2018GL079759>
- 1017 Plaut, J.J., Safaeinili, A., Holt, J.W., Phillips, R.J., Head, J.W., Seu, R., Putzig, N.E., Frigeri, A., 2009.
1018 Radar evidence for ice in lobate debris aprons in the mid-northern latitudes of Mars.
1019 *Geophys. Res. Lett.* 36, 02203. <https://doi.org/10.1029/2008GL036379>
- 1020 Pollack, J.B., Kasting, J.F., Richardson, S.M., Poliakoff, K., 1987. The case for a wet, warm climate on
1021 early Mars. *Icarus* 71, 203–224. [https://doi.org/10.1016/0019-1035\(87\)90147-3](https://doi.org/10.1016/0019-1035(87)90147-3)
- 1022 Porco, C.C., Baker, E., Barbara, J., Beurle, K., Brahic, A., Burns, J.A., Charnoz, S., Cooper, N., Dawson,
1023 D.D., Del Genio, A.D., Denk, T., Dones, L., Dyudina, U., Evans, M.W., Fussner, S., Giese, B.,
1024 Grazier, K., Helfenstein, P., Ingwersoll, A.P., Jacobson, R.A., Johnson, T.V., McEwen, A., Murray,
1025 C.D., Neukum, G., Owen, W.M., Perry, J., Roatsch, T., Spitale, J., Squyres, S., Thomas, P.,
1026 Tiscareno, M., Turtle, E.P., Vasavada, A.R., Veverka, J., Wagner, R., West, R., 2005. Imaging of
1027 Titan from the Cassini spacecraft. *Nature* 434, 159–168.
1028 <https://doi.org/10.1038/nature03436>
- 1029 Portyankina, G., Markiewicz, W.J., Thomas, N., Hansen, C.J., Milazzo, M., 2010. HiRISE observations of
1030 gas sublimation-driven activity in Mars' southern polar regions: III. Models of processes
1031 involving translucent ice. *MROHiRISE Stud. Mars* 205, 311–320.
1032 <https://doi.org/10.1016/j.icarus.2009.08.029>
- 1033 Poulos, M.J., Pierce, J.L., Flores, A.N., Benner, S.G., 2012. Hillslope asymmetry maps reveal
1034 widespread, multi-scale organization: MAPPING HILLSLOPE ASYMMETRY. *Geophys. Res. Lett.*
1035 39, n/a-n/a. <https://doi.org/10.1029/2012GL051283>

- 1036 Quantin, C., Flahaut, J., Clenet, H., Allemand, P., Thomas, P., 2012. Composition and structures of the
1037 subsurface in the vicinity of Valles Marineris as revealed by central uplifts of impact craters.
1038 *Icarus* 221, 436–452. <https://doi.org/10.1016/j.icarus.2012.07.031>
- 1039 Reiss, D., Raack, J., Rossi, A.P., Di Achille, G., Hiesinger, H., 2010. First in-situ analysis of dust devil
1040 tracks on Earth and their comparison with tracks on Mars: DARK DUST DEVIL TRACKS ON
1041 EARTH. *Geophys. Res. Lett.* 37, n/a-n/a. <https://doi.org/10.1029/2010GL044016>
- 1042 Roberts, G.P., Matthews, B., Bristow, C., Guerrieri, L., Vetterlein, J., 2012. Possible evidence of
1043 paleomarsquakes from fallen boulder populations, Cerberus Fossae, Mars. *J. Geophys. Res.*
1044 *Planets* 117, E02009. <https://doi.org/10.1029/2011JE003816>
- 1045 Rodriguez, J.A.P., Fairén, A.G., Tanaka, K.L., Zarroca, M., Linares, R., Platz, T., Komatsu, G., Miyamoto,
1046 H., Kargel, J.S., Yan, J., Gulick, V., Higuchi, K., Baker, V.R., Glines, N., 2016. Tsunami waves
1047 extensively resurfaced the shorelines of an early Martian ocean. *Sci. Rep.* 6, 25106.
1048 <https://doi.org/10.1038/srep25106>
- 1049 Rodriguez, J.A.P., Leonard, G.J., Kargel, J.S., Domingue, D., Berman, D.C., Banks, M., Zarroca, M.,
1050 Linares, R., Marchi, S., Baker, V.R., Webster, K.D., Sykes, M., 2020. The Chaotic Terrains of
1051 Mercury Reveal a History of Planetary Volatile Retention and Loss in the Innermost Solar
1052 System. *Sci. Rep.* 10, 4737. <https://doi.org/10.1038/s41598-020-59885-5>
- 1053 Ruesch, O., Sefton-Nash, E., Vago, J.L., Küppers, M., Pasckert, J.H., Krohn, K., Otto, K., 2020. In situ
1054 fragmentation of lunar blocks and implications for impacts and solar-induced thermal
1055 stresses. *Icarus* 336, 113431. <https://doi.org/10.1016/j.icarus.2019.113431>
- 1056 Ryan, J.A., Lucich, R.D., 1983. Possible dust devils, vortices on Mars. *J. Geophys. Res.* 88, 11005.
1057 <https://doi.org/10.1029/JC088iC15p11005>
- 1058 Sasaki, S., Honda, C., Sugita, S., Miyamoto, H., Michikami, T., Morota, T., Kanda, S., Kikuchi, H.,
1059 2021. Crack orientations of boulders and thermal fatigue on (162173) Ryugu. 43rd COSPAR
1060 Sci. Assem. Held 28 January-4 Febr. 43, 270.
- 1061 Sauro, F., Pozzobon, R., Massironi, M., De Berardinis, P., Santagata, T., De Waele, J., 2020. Lava tubes
1062 on Earth, Moon and Mars: A review on their size and morphology revealed by comparative
1063 planetology. *Earth-Sci. Rev.* 209, 103288. <https://doi.org/10.1016/j.earscirev.2020.103288>
- 1064 Schenk, P., Jackson, M.P.A., 1993. Diapirism on Triton: A record of crustal layering and instability.
1065 *Geology* 21, 299–302.
- 1066 Schleicher, L.S., Watters, T.R., Martin, A.J., Banks, M.E., 2019. Wrinkle ridges on Mercury and the
1067 Moon within and outside of mascons. *Icarus* 331, 226–237.
1068 <https://doi.org/10.1016/j.icarus.2019.04.013>
- 1069 Schmidt, B.E., Hughson, K.H.G., Chilton, H.T., Scully, J.E.C., Platz, T., Nathues, A., Sizemore, H., Bland,
1070 M.T., Byrne, S., Marchi, S., O'Brien, D.P., Schorghofer, N., Hiesinger, H., Jaumann, R.,
1071 Pasckert, J.H., Lawrence, J.D., Buzkowski, D., Castillo-Rogez, J.C., Sykes, M.V., Schenk, P.M.,
1072 De Sanctis, M.-C., Mitri, G., Formisano, M., Li, J.-Y., Reddy, V., LeCorre, L., Russell, C.T.,
1073 Raymond, C.A., 2017. Geomorphological evidence for ground ice on dwarf planet Ceres. *Nat. Geosci.* 10, 338–343. <https://doi.org/10.1038/ngeo2936>
- 1075 Schmidt, F., Andrieu, F., Costard, F., Kocifaj, M., Meresescu, A.G., 2017. Formation of recurring slope
1076 lineae on Mars by rarefied gas-triggered granular flows. *Nat. Geosci.* 10, 270–273.
- 1077 Schorghofer, N., Aharonson, O., Gerstell, M.F., Tatsumi, L., 2007. Three decades of slope streak
1078 activity on Mars. *Icarus* 191, 132–140. <https://doi.org/10.1016/j.icarus.2007.04.026>
- 1079 Schultz, P.H., Gault, D.E., 1975. Seismic effects from major basin formations on the moon and
1080 mercury. *The Moon* 12, 159–177. <https://doi.org/10.1007/BF00577875>
- 1081 Scully, J.E.C., Russell, C.T., Yin, A., Jaumann, R., Carey, E., Castillo-Rogez, J., McSween, H.Y., Raymond,
1082 C.A., Reddy, V., Le Corre, L., 2015. Geomorphological evidence for transient water flow on
1083 Vesta. *Earth Planet. Sci. Lett.* 411, 151–163. <https://doi.org/10.1016/j.epsl.2014.12.004>
- 1084 Sefton-Nash, E., Catling, D.C., Wood, S.E., Grindrod, P.M., Teanby, N.A., 2012. Topographic, spectral
1085 and thermal inertia analysis of interior layered deposits in Iani Chaos, Mars. *Icarus* 221, 20–
1086 42. <https://doi.org/10.1016/j.icarus.2012.06.036>

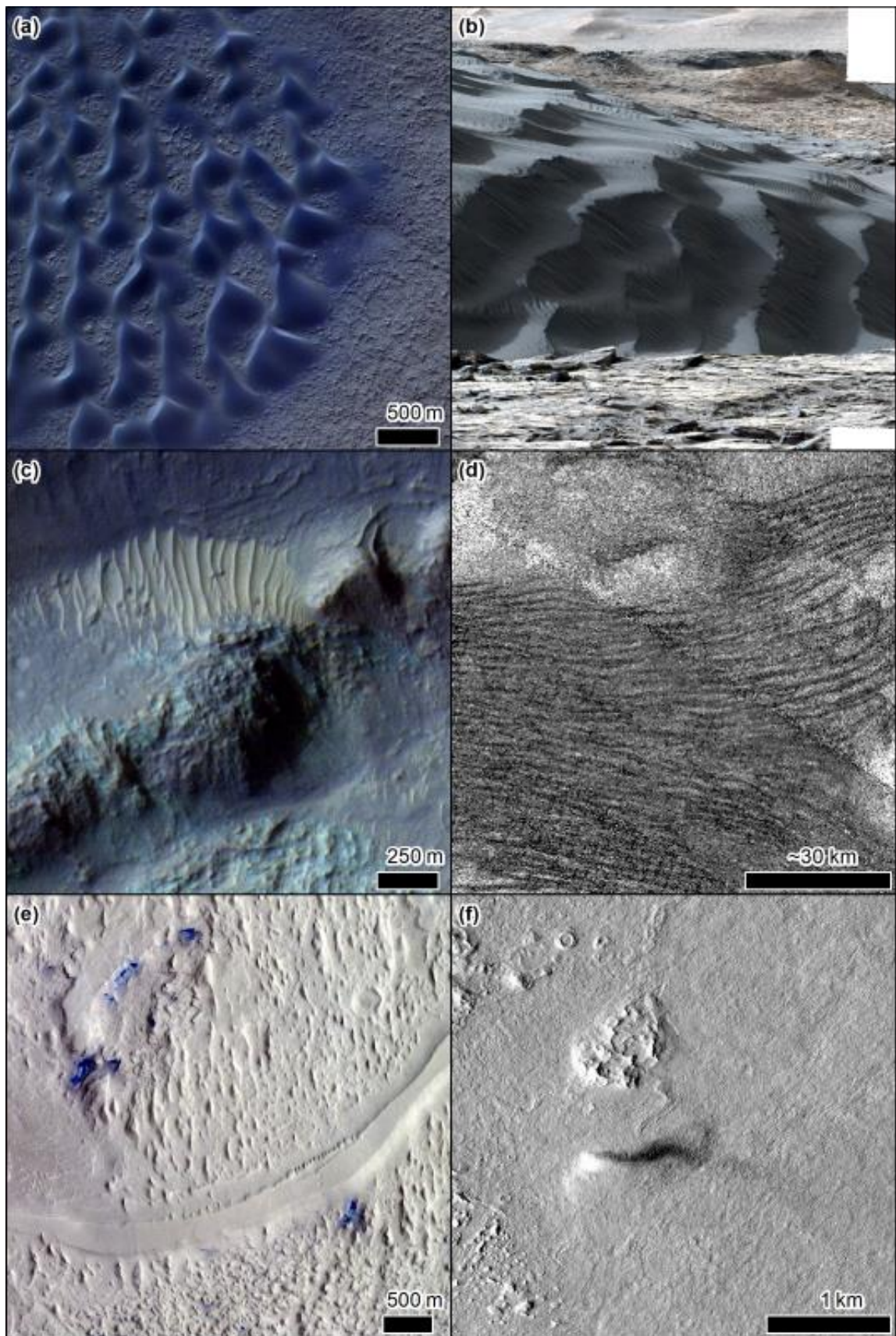
- 1087 Séjourné, A., Costard, F., Gargani, J., Soare, R.J., Fedorov, A., Marmo, C., 2011. Scalloped depressions
1088 and small-sized polygons in western Utopia Planitia, Mars: A new formation hypothesis.
1089 *Planet. Space Sci.* 59, 412–422. <https://doi.org/10.1016/j.pss.2011.01.007>
- 1090 Senthil Kumar, P., Keerthi, V., Senthil Kumar, A., Mustard, J., Gopala Krishna, B., Amitabh, Ostrach,
1091 L.R., Kring, David.A., Kiran Kumar, A.S., Goswami, J.N., 2013. Gullies and landslides on the
1092 Moon: Evidence for dry-granular flows. *J. Geophys. Res. Planets* 118, 206–223.
1093 <https://doi.org/10.1002/jgre.20043>
- 1094 Senthil Kumar, P., Sruthi, U., Krishna, N., Lakshmi, K.J.P., Menon, R., Amitabh, Gopala Krishna, B.,
1095 Kring, D.A., Head, J.W., Goswami, J.N., Kiran Kumar, A.S., 2016. Recent shallow moonquake
1096 and impact-triggered boulder falls on the Moon: New insights from the Schrödinger basin:
1097 Recent Seismotectonics of the Moon. *J. Geophys. Res. Planets*.
1098 <https://doi.org/10.1002/2015JE004850>
- 1099 Sharp, R.P., 1980. Geomorphological Processes on Terrestrial Planetary Surfaces. *Annu. Rev. Earth*
1100 *Planet. Sci.* 8, 231–261. <https://doi.org/10.1146/annurev.ea.08.050180.001311>
- 1101 Sholes, S.F., Dickeson, Z.I., Montgomery, D.R., Catling, D.C., 2021. Where are Mars' Hypothesized
1102 Ocean Shorelines? Large Lateral and Topographic Offsets Between Different Versions of
1103 Paleoshoreline Maps. *J. Geophys. Res. Planets* 126. <https://doi.org/10.1029/2020JE006486>
- 1104 Singer, K.N., McKinnon, W.B., Schenk, P.M., Moore, J.M., 2012. Massive ice avalanches on Iapetus
1105 mobilized by friction reduction during flash heating. *Nat. Geosci.* 5, 574–578.
1106 <https://doi.org/10.1038/ngeo1526>
- 1107 Skjetne, H.L., Singer, K.N., Hynek, B.M., Knight, K.I., Schenk, P.M., Olkin, C.B., White, O.L., Bertrand,
1108 T., Runyon, K.D., McKinnon, W.B., Moore, J.M., Stern, S.A., Weaver, H.A., Young, L.A., Ennico,
1109 K., 2021. Morphological comparison of blocks in chaos terrains on Pluto, Europa, and Mars.
1110 *Icarus* 356, 113866. <https://doi.org/10.1016/j.icarus.2020.113866>
- 1111 Soare, R.J., Burr, D.M., Wan Bun Tseung, J.M., 2005. Possible pingos and a periglacial landscape in
1112 northwest Utopia Planitia. *Icarus* 174, 373–382. <https://doi.org/10.1016/j.icarus.2004.11.013>
- 1113 Soare, R.J., Conway, S.J., Dohm, J.M., 2014. Possible ice-wedge polygons and recent landscape
1114 modification by “wet” periglacial processes in and around the Argyre impact basin, Mars.
1115 *Icarus* 233, 214–228. <https://doi.org/10.1016/j.icarus.2014.01.034>
- 1116 Soare, R.J., Conway, S.J., Gallagher, C., Dohm, J.M., 2016. Sorted (clastic) polygons in the Argyre
1117 region, Mars, and possible evidence of pre- and post-glacial periglaciation in the Late
1118 Amazonian Epoch. *Icarus* 264, 184–197. <https://doi.org/10.1016/j.icarus.2015.09.019>
- 1119 Soare, R.J., Conway, S.J., Williams, J.-P., Philippe, M., Mc Keown, L.E., Godin, E., Hawkswell, J., 2021.
1120 Possible ice-wedge polygonisation in Utopia Planitia, Mars and its latitudinal gradient of
1121 distribution. *Icarus* 358, 114208. <https://doi.org/10.1016/j.icarus.2020.114208>
- 1122 Soare, R.J., Kargel, J.S., Osinski, G.R., Costard, F., 2007. Thermokarst processes and the origin of
1123 crater-rim gullies in Utopia and western Elysium Planitia. *Icarus* 191, 95–112.
- 1124 Soare, R.J., Osinski, G.R., Roehm, C.L., 2008. Thermokarst lakes and ponds on Mars in the very recent
1125 (late Amazonian) past. *Earth Planet. Sci. Lett.* 272, 382–393.
1126 <https://doi.org/10.1016/j.epsl.2008.05.010>
- 1127 Soderblom, L.A., 1970. A model for small-impact erosion applied to the lunar surface. *J. Geophys.*
1128 *Res.* 75, 2655–2661. <https://doi.org/10.1029/JB075i014p02655>
- 1129 Stein, N., Grotzinger, J.P., Schieber, J., Mangold, N., Hallet, B., Newsom, H., Stack, K.M., Berger, J.A.,
1130 Thompson, L., Siebach, K.L., Cousin, A., Le Mouélic, S., Minitti, M., Sumner, D.Y., Fedo, C.,
1131 House, C.H., Gupta, S., Vasavada, A.R., Gellert, R., Wiens, R.C., Frydenvang, J., Forni, O.,
1132 Meslin, P.Y., Payré, V., Dehouck, E., 2018. Desiccation cracks provide evidence of lake drying
1133 on Mars, Sutton Island member, Murray formation, Gale Crater. *Geology* 46, 515–518.
1134 <https://doi.org/10.1130/G40005.1>
- 1135 Stern, S.A., Binzel, R.P., Earle, A.M., Singer, K.N., Young, L.A., Weaver, H.A., Olkin, C.B., Ennico, K.,
1136 Moore, J.M., McKinnon, W.B., Spencer, J.R., 2017. Past epochs of significantly higher
1137 pressure atmospheres on Pluto. *Icarus* 287, 47–53.
1138 <https://doi.org/10.1016/j.icarus.2016.11.022>

- 1139 Stillman, D.E., Bue, B.D., Wagstaff, K.L., Primm, K.M., Michaels, T.I., Grimm, R.E., 2020. Evaluation of
1140 wet and dry recurring slope lineae (RSL) formation mechanisms based on quantitative
1141 mapping of RSL in Garni Crater, Valles Marineris, Mars. *Icarus* 335, 113420.
1142 <https://doi.org/10.1016/j.icarus.2019.113420>
- 1143 Stuart-Alexander, D.E., Howard, K.A., 1970. Lunar Maria and circular basins—a review. *Icarus* 12,
1144 440–456. [https://doi.org/10.1016/0019-1035\(70\)90013-8](https://doi.org/10.1016/0019-1035(70)90013-8)
- 1145 Sullivan, R., Kok, J.F., Katra, I., Yizhaq, H., 2020. A Broad Continuum of Aeolian Impact Ripple
1146 Morphologies on Mars is Enabled by Low Wind Dynamic Pressures. *J. Geophys. Res. Planets*
1147 125. <https://doi.org/10.1029/2020JE006485>
- 1148 Sullivan, R., Thomas, P., Veverka, J., Malin, M., Edgett, K.S., 2001. Mass movement slope streaks
1149 imaged by the Mars Orbiter Camera. *J Geophys Res-Planets* 106, 23607–23633.
- 1150 Telfer, M.W., Parteli, E.J.R., Radebaugh, J., Beyer, R.A., Bertrand, T., Forget, F., Nimmo, F., Grundy,
1151 W.M., Moore, J.M., Stern, S.A., Spencer, J., Lauer, T.R., Earle, A.M., Binzel, R.P., Weaver, H.A.,
1152 Olkin, C.B., Young, L.A., Ennico, K., Runyon, K., The New Horizons Geology, Geophysics and
1153 Imaging Science Theme Team, Buie, M., Buratti, B., Cheng, A., Kavelaars, J.J., Linscott, I.,
1154 McKinnon, W.B., Reitsema, H., Reuter, D., Schenk, P., Showalter, M., Tyler, L., 2018. Dunes on
1155 Pluto. *Science* 360, 992–997. <https://doi.org/10.1126/science.aao2975>
- 1156 Tesson, P.-A., Conway, S.J., Mangold, N., Ciazela, J., Lewis, S.R., Mège, D., 2020. Evidence for thermal-
1157 stress-induced rockfalls on Mars impact crater slopes. *Icarus* 342, 113503.
1158 <https://doi.org/10.1016/j.icarus.2019.113503>
- 1159 Thomas, N., Davidsson, B., El-Maarry, M.R., Fornasier, S., Giacomini, L., Gracia-Berná, A.G., Hviid, S.F.,
1160 Ip, W.-H., Jorda, L., Keller, H.U., Knollenberg, J., Kührt, E., La Forgia, F., Lai, I.L., Liao, Y.,
1161 Marschall, R., Massironi, M., Mottola, S., Pajola, M., Poch, O., Pommerol, A., Preusker, F.,
1162 Scholten, F., Su, C.C., Wu, J.S., Vincent, J.-B., Sierks, H., Barbieri, C., Lamy, P.L., Rodrigo, R.,
1163 Koschny, D., Rickman, H., A'Hearn, M.F., Barucci, M.A., Bertaux, J.-L., Bertini, I., Cremonese,
1164 G., Da Deppo, V., Debei, S., de Cecco, M., Fulle, M., Groussin, O., Gutierrez, P.J., Kramm, J.-R.,
1165 Küppers, M., Lara, L.M., Lazzarin, M., Lopez Moreno, J.J., Marzari, F., Michalik, H., Naletto, G.,
1166 Agarwal, J., Güttler, C., Oklay, N., Tubiana, C., 2015. Redistribution of particles across the
1167 nucleus of comet 67P/Churyumov-Gerasimenko. *Astron. Astrophys.* 583, A17.
1168 <https://doi.org/10.1051/0004-6361/201526049>
- 1169 Thomas, N., Portyankina, G., Hansen, C.J., Pommerol, A., 2011. HiRISE observations of gas
1170 sublimation-driven activity in Mars' southern polar regions: IV. Fluid dynamics models of CO₂
1171 jets. *Icarus* 212, 66–85. <https://doi.org/10.1016/j.icarus.2010.12.016>
- 1172 Thomas, P., Giersch, P.J., 1985. Dust Devils on Mars. *Science* 230, 175–177.
1173 <https://doi.org/10.1126/science.230.4722.175>
- 1174 Thomas, R.J., Rothery, D.A., Conway, S.J., Anand, M., 2014. Long-lived explosive volcanism on
1175 Mercury. *Geophys. Res. Lett.* 41, 6084–6092. <https://doi.org/10.1002/2014GL061224>
- 1176 Thomson, B.J., Bridges, N.T., Greeley, R., 2008. Rock abrasion features in the Columbia Hills, Mars. *J.*
1177 *Geophys. Res.* 113, E08010. <https://doi.org/10.1029/2007JE003018>
- 1178 Tomasko, M.G., Archinal, B., Becker, T., Bézard, B., Bushroe, M., Combes, M., Cook, D., Coustenis, A.,
1179 de Bergh, C., Dafoe, L.E., Doose, L., Douté, S., Eibl, A., Engel, S., Gliem, F., Grieger, B., Holso,
1180 K., Howington-Kraus, E., Karkoschka, E., Keller, H.U., Kirk, R., Kramm, R., Küppers, M.,
1181 Lanagan, P., Lellouch, E., Lemmon, M., Lunine, J., McFarlane, E., Moores, J., Prout, G.M., Rizk,
1182 B., Rosiek, M., Rueffer, P., Schröder, S.E., Schmitt, B., See, C., Smith, P., Soderblom, L.,
1183 Thomas, N., West, R., 2005. Rain, winds and haze during the Huygens probe's descent to
1184 Titan's surface. *Nature* 438, 765–778. <https://doi.org/10.1038/nature04126>
- 1185 van den Broeke, M.R., Bintanja, R., 1995. Summertime atmospheric circulation in the vicinity of a
1186 blue ice area in Queen Maud Land, Antarctica. *Bound.-Layer Meteorol.* 72, 411–438.
1187 <https://doi.org/10.1007/BF00709002>
- 1188 Veeder, G.J., Davies, A.G., Matson, D.L., Johnson, T.V., 2009. Io: Heat flow from dark volcanic fields.
1189 *Icarus* 204, 239–253. <https://doi.org/10.1016/j.icarus.2009.06.027>

- 1190 Vijayan, S., Harish, Kimi, K., Tuhi, S., Vigneshwaran, K., Sinha, R., Conway, S.J., Sivaraman, B.,
1191 Bhardwaj, A., 2021. Boulder Fall Ejecta: Present day activity on Mars. *Geophys. Res. Lett.*
1192 Accepted.
1193 Vincent, J.-B., Bodewits, D., Besse, S., Sierks, H., Barbieri, C., Lamy, P., Rodrigo, R., Koschny, D.,
1194 Rickman, H., Keller, H.U., Agarwal, J., A'Hearn, M.F., Auger, A.-T., Barucci, M.A., Bertaux, J.-L.,
1195 Bertini, I., Capanna, C., Cremonese, G., Da Deppo, V., Davidsson, B., Debei, S., De Cecco, M.,
1196 El-Maarry, M.R., Ferri, F., Fornasier, S., Fulle, M., Gaskell, R., Giacomini, L., Groussin, O.,
1197 Guilbert-Lepoutre, A., Gutierrez-Marques, P., Gutierrez, P.J., Guttler, C., Hoekzema, N.,
1198 Hofner, S., Hviid, S.F., Ip, W.-H., Jorda, L., Knollenberg, J., Kovacs, G., Kramm, R., Kuhrt, E.,
1199 Kuppers, M., La Forgia, F., Lara, L.M., Lazzarin, M., Lee, V., Leyrat, C., Lin, Z.-Y., Lopez Moreno,
1200 J.J., Lowry, S., Magrin, S., Maquet, L., Marchi, S., Marzari, F., Massironi, M., Michalik, H.,
1201 Moissl, R., Mottola, S., Naletto, G., Oklay, N., Pajola, M., Preusker, F., Scholten, F., Thomas,
1202 N., Toth, I., Tubiana, C., 2015. Large heterogeneities in comet 67P as revealed by active pits
1203 from sinkhole collapse. *Nature* 523, 63–66. <https://doi.org/10.1038/nature14564>
1204 Vincent, J.-B., Oklay, N., Pajola, M., Höfner, S., Sierks, H., Hu, X., Barbieri, C., Lamy, P.L., Rodrigo, R.,
1205 Koschny, D., Rickman, H., Keller, H.U., A'Hearn, M.F., Barucci, M.A., Bertaux, J.-L., Bertini, I.,
1206 Besse, S., Bodewits, D., Cremonese, G., Da Deppo, V., Davidsson, B., Debei, S., De Cecco, M.,
1207 El-Maarry, M.R., Fornasier, S., Fulle, M., Groussin, O., Gutiérrez, P.J., Gutiérrez-Marquez, P.,
1208 Gütler, C., Hofmann, M., Hviid, S.F., Ip, W.-H., Jorda, L., Knollenberg, J., Kovacs, G., Kramm,
1209 J.-R., Kührt, E., Küppers, M., Lara, L.M., Lazzarin, M., Lin, Z.-Y., Lopez Moreno, J.J., Lowry, S.,
1210 Marzari, F., Massironi, M., Moreno, F., Mottola, S., Naletto, G., Preusker, F., Scholten, F., Shi,
1211 X., Thomas, N., Toth, I., Tubiana, C., 2016. Are fractured cliffs the source of cometary dust
1212 jets? Insights from OSIRIS/Rosetta at 67P/Churyumov-Gerasimenko. *Astron. Astrophys.* 587,
1213 A14. <https://doi.org/10.1051/0004-6361/201527159>
1214 Viola, D., McEwen, A.S., Dundas, C.M., Byrne, S., 2015. Expanded secondary craters in the Arcadia
1215 Planitia region, Mars: Evidence for tens of Myr-old shallow subsurface ice. *Icarus* 248, 190–
1216 204. <https://doi.org/10.1016/j.icarus.2014.10.032>
1217 Walsh, K.J., Jawin, E.R., Ballouz, R.-L., Barnouin, O.S., Bierhaus, E.B., Connolly, H.C., Molaro, J.L.,
1218 McCoy, T.J., Delbo', M., Hartzell, C.M., Pajola, M., Schwartz, S.R., Trang, D., Asphaug, E.,
1219 Becker, K.J., Beddingfield, C.B., Bennett, C.A., Bottke, W.F., Burke, K.N., Clark, B.C., Daly,
1220 M.G., DellaGiustina, D.N., Dworkin, J.P., Elder, C.M., Golish, D.R., Hildebrand, A.R., Malhotra,
1221 R., Marshall, J., Michel, P., Nolan, M.C., Perry, M.E., Rizk, B., Ryan, A., Sandford, S.A.,
1222 Scheeres, D.J., Susorney, H.C.M., Thuillet, F., Lauretta, D.S., The OSIRIS-REx Team, 2019.
1223 Craters, boulders and regolith of (101955) Bennu indicative of an old and dynamic surface.
1224 *Nat. Geosci.* 12, 242–246. <https://doi.org/10.1038/s41561-019-0326-6>
1225 Warner, N., Gupta, S., Muller, J.-P., Kim, J.-R., Lin, S.-Y., 2009. A refined chronology of catastrophic
1226 outflow events in Ares Vallis, Mars. *Earth Planet. Sci. Lett.* 288, 58–69.
1227 Watters, T.R., Robinson, M.S., Beyer, R.A., Banks, M.E., Bell, J.F., Pritchard, M.E., Hiesinger, H., van
1228 der Bogert, C.H., Thomas, P.C., Turtle, E.P., Williams, N.R., 2010. Evidence of Recent Thrust
1229 Faulting on the Moon Revealed by the Lunar Reconnaissance Orbiter Camera. *Science* 329,
1230 936–940. <https://doi.org/10.1126/science.1189590>
1231 Wells, G.L., Zimbelman, J.R., 1997. Extraterrestrial arid surface processes. *Arid Zone Geomorphol.*
1232 Process Form Change Drylands.
1233 White, O.L., Umurhan, O.M., Moore, J.M., Howard, A.D., 2016. Modeling of ice pinnacle formation on
1234 Callisto: Modeling of Callisto's Pinnacle Terrain. *J. Geophys. Res. Planets* 121, 21–45.
1235 <https://doi.org/10.1002/2015JE004846>
1236 Williams, R.M.E., Grotzinger, J.P., Dietrich, W.E., Gupta, S., Sumner, D.Y., Wiens, R.C., Mangold, N.,
1237 Malin, M.C., Edgett, K.S., Maurice, S., Forni, O., Gasnault, O., Olliila, A., Newsom, H.E.,
1238 Dromart, G., Palucis, M.C., Yingst, R.A., Anderson, R.B., Herkenhoff, K.E., Le Mouelic, S.,
1239 Goetz, W., Madsen, M.B., Koefoed, A., Jensen, J.K., Bridges, J.C., Schwenzer, S.P., Lewis, K.W.,
1240 Stack, K.M., Rubin, D., Kah, L.C., Bell, J.F., Farmer, J.D., Sullivan, R., Van Beek, T., Blaney, D.L.,
1241 Pariser, O., Deen, R.G., MSL Science Team, Kemppinen, O., Bridges, N., Johnson, J.R., Miniti,

1242 M., Cremers, D., Edgar, L., Godber, A., Wadhwa, M., Wellington, D., McEwan, I., Newman, C.,
1243 Richardson, M., Charpentier, A., Peret, L., King, P., Blank, J., Weigle, G., Schmidt, M., Li, S.,
1244 Milliken, R., Robertson, K., Sun, V., Baker, M., Edwards, C., Ehlmann, B., Farley, K., Griffes, J.,
1245 Miller, H., Newcombe, M., Pilorget, C., Rice, M., Siebach, K., Stolper, E., Brunet, C., Hipkin, V.,
1246 Leveille, R., Marchand, G., Sobron Sanchez, P., Favot, L., Cody, G., Steele, A., Fluckiger, L.,
1247 Lees, D., Nefian, A., Martin, M., Gailhanou, M., Westall, F., Israel, G., Agard, C., Baroukh, J.,
1248 Donny, C., Gaboriaud, A., Guillemot, P., Lafaille, V., Lorigny, E., Paillet, A., Perez, R., Saccoccio,
1249 M., Yana, C., Aparicio, C.A., Caride Rodriguez, J., Carrasco Blazquez, I., Gomez Gomez, F.,
1250 Elvira, J.G., Hettrich, S., Lepinette Malvitte, A., Marin Jimenez, M., Frias, J.M., Soler, J.M.,
1251 Torres, F.J.M., Molina Jurado, A., Sotomayor, L.M., Munoz Caro, G., Navarro Lopez, S.,
1252 Gonzalez, V.P., Garcia, J.P., Rodriguez Manfredi, J.A., Planello, J.J.R., Alejandra Sans Fuentes,
1253 S., Sebastian Martinez, E., Torres Redondo, J., O'Callaghan, R.U., Zorzano Mier, M.-P.,
1254 Chipera, S., Lacour, J.-L., Mauchien, P., Sirven, J.-B., Manning, H., Fairen, A., Hayes, A.,
1255 Joseph, J., Squyres, S., Thomas, P., Dupont, A., Lundberg, A., Melikechi, N., Mezzacappa, A.,
1256 DeMarines, J., Grinspoon, D., Reitz, G., Prats, B., Atlaskin, E., Genzer, M., Harri, A.-M.,
1257 Haukka, H., Kahanpaa, H., Kauhanen, J., Paton, M., Polkko, J., Schmidt, W., Siili, T., Fabre, C.,
1258 Wray, J., Wilhelm, M.B., Poitrasson, F., Patel, K., Gorevan, S., Indyk, S., Paulsen, G., Bish, D.,
1259 Schieber, J., Gondet, B., Langevin, Y., Geffroy, C., Baratoux, D., Berger, G., Cros, A., Uston, C.,
1260 d., Lasue, J., Lee, Q.-M., Meslin, P.-Y., Pallier, E., Parot, Y., Pinet, P., Schroder, S., Toplis, M.,
1261 Lewin, E., Brunner, W., Heydari, E., Achilles, C., Oehler, D., Sutter, B., Cabane, M., Coscia, D.,
1262 Szopa, C., Robert, F., Sautter, V., Nachon, M., Buch, A., Stalport, F., Coll, P., Francois, P.,
1263 Raulin, F., Teinturier, S., Cameron, J., Clegg, S., Cousin, A., DeLapp, D., Dingler, R., Jackson,
1264 R.S., Johnstone, S., Lanza, N., Little, C., Nelson, T., Williams, R.B., Jones, A., Kirkland, L.,
1265 Treiman, A., Baker, B., Cantor, B., Caplinger, M., Davis, S., Duston, B., Fay, D., Hardgrove, C.,
1266 Harker, D., Herrera, P., Jensen, E., Kennedy, M.R., Krezoski, G., Krysak, D., Lipkaman, L.,
1267 McCartney, E., McNair, S., Nixon, B., Posiolova, L., Ravine, M., Salamon, A., Saper, L., Stoiber,
1268 K., Supulver, K., Van Beek, J., Zimdar, R., French, K.L., Iagnemma, K., Miller, K., Summons, R.,
1269 Goesmann, F., Hviid, S., Johnson, M., Lefavor, M., Lyness, E., Breves, E., Dyar, M.D., Fassett,
1270 C., Blake, D.F., Bristow, T., DesMarais, D., Edwards, L., Haberle, R., Hoehler, T., Hollingsworth,
1271 J., Kahre, M., Keely, L., McKay, C., Bleacher, L., Brinckerhoff, W., Choi, D., Conrad, P.,
1272 Dworkin, J.P., Eigenbrode, J., Floyd, M., Freissinet, C., Garvin, J., Glavin, D., Harpold, D.,
1273 Mahaffy, P., Martin, D.K., McAdam, A., Pavlov, A., Raaen, E., Smith, M.D., Stern, J., Tan, F.,
1274 Trainer, M., Meyer, M., Posner, A., Voytek, M., Anderson, R.C., Aubrey, A., Beegle, L.W.,
1275 Behar, A., Brinza, D., Calef, F., Christensen, L., Crisp, J.A., DeFlores, L., Feldman, J., Feldman,
1276 S., Flesch, G., Hurowitz, J., Jun, I., Keymeulen, D., Maki, J., Mischna, M., Morookian, J.M.,
1277 Parker, T., Pavri, B., Schoppers, M., Sengstacken, A., Simmonds, J.J., Spanovich, N., de la
1278 Torre Juarez, M., Vasavada, A.R., Webster, C.R., Yen, A., Archer, P.D., Cucinotta, F., Jones,
1279 J.H., Ming, D., Morris, R.V., Niles, P., Rampe, E., Nolan, T., Fisk, M., Radziemski, L.,
1280 Barraclough, B., Bender, S., Berman, D., Dobrea, E.N., Tokar, R., Vaniman, D., Leshin, L.,
1281 Cleghorn, T., Huntress, W., Manhes, G., Hudgins, J., Olson, T., Stewart, N., Sarrazin, P., Grant,
1282 J., Vicenzi, E., Wilson, S.A., Bullock, M., Ehresmann, B., Hamilton, V., Hassler, D., Peterson, J.,
1283 Rafkin, S., Zeitlin, C., Fedosov, F., Golovin, D., Karpushkina, N., Kozyrev, A., Litvak, M.,
1284 Malakhov, A., Mitrofanov, I., Mokrousov, M., Nikiforov, S., Prokhorov, V., Sanin, A.,
1285 Tretyakov, V., Varenikov, A., Vosstrukhin, A., Kuzmin, R., Clark, B., Wolff, M., McLennan, S.,
1286 Botta, O., Drake, D., Bean, K., Lemmon, M., Lee, E.M., Sucharski, R., Hernandez, M.A. d. P.,
1287 Blanco Avalos, J.J., Ramos, M., Kim, M.-H., Malespin, C., Plante, I., Muller, J.-P., Gonzalez,
1288 R.N., Ewing, R., Boynton, W., Downs, R., Fitzgibbon, M., Harshman, K., Morrison, S.,
1289 Kortmann, O., Williams, A., Lugmair, G., Wilson, M.A., Jakosky, B., Zunic, T.B., Frydenvang, J.,
1290 Kinch, K., Stipp, S.L.S., Boyd, N., Campbell, J.L., Gellert, R., Perrett, G., Pradler, I., VanBommel,
1291 S., Jacob, S., Owen, T., Rowland, S., Savijarvi, H., Boehm, E., Bottcher, S., Burmeister, S., Guo,
1292 J., Kohler, J., Garcia, C.M., Mellin, R.M., Schweingruber, R.W., McConnochie, T., Benna, M.,
1293 Franz, H., Bower, H., Brunner, A., Blau, H., Boucher, T., Carmosino, M., Atreya, S., Elliott, H.,

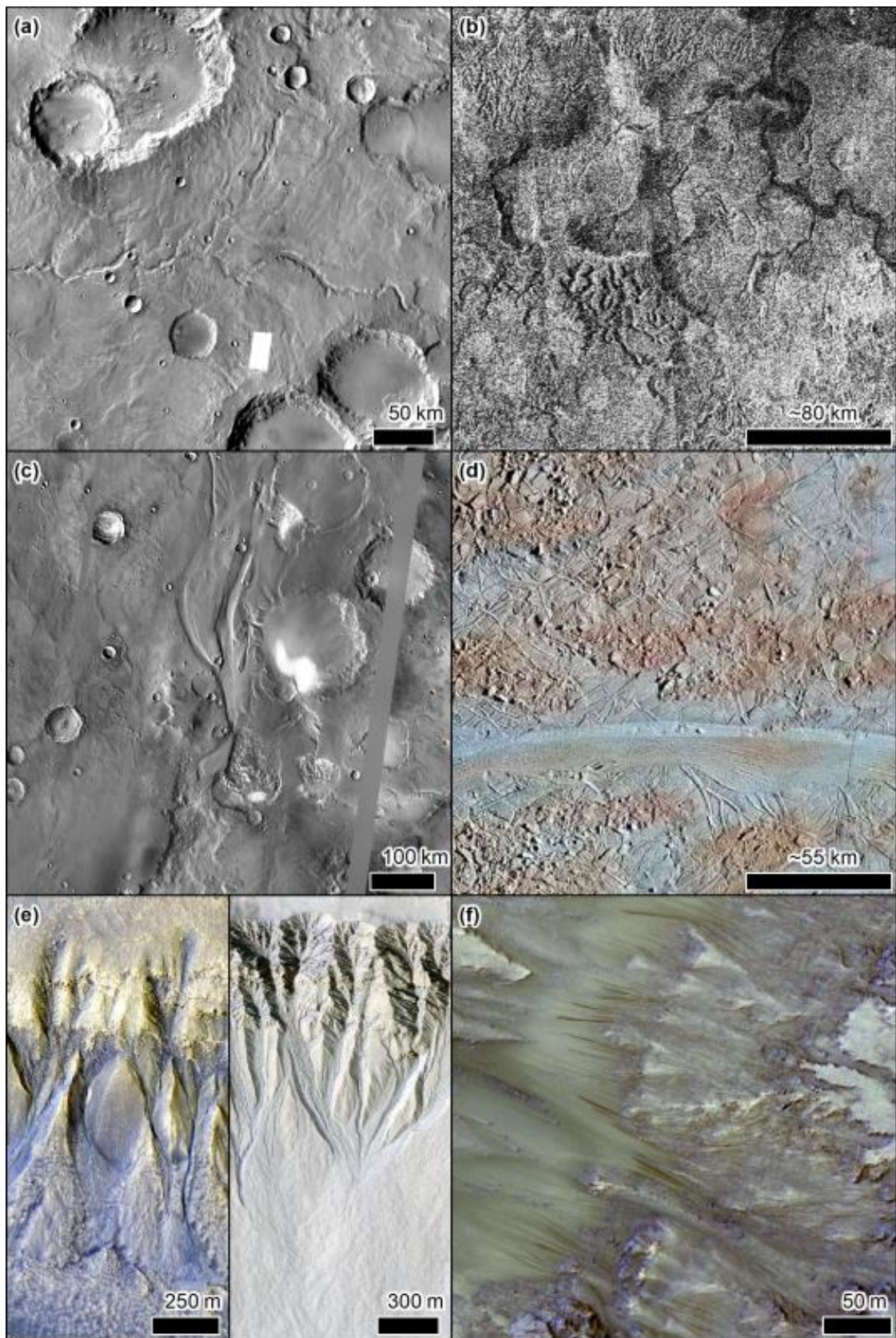
- 1294 Halleaux, D., Renno, N., Wong, M., Pepin, R., Elliott, B., Spray, J., Thompson, L., Gordon, S.,
1295 Williams, J., Vasconcelos, P., Bentz, J., Nealson, K., Popa, R., Moersch, J., Tate, C., Day, M.,
1296 Kocurek, G., Hallet, B., Sletten, R., Francis, R., McCullough, E., Cloutis, E., ten Kate, I.L.,
1297 Arvidson, R., Fraeman, A., Scholes, D., Slavney, S., Stein, T., Ward, J., Berger, J., Moores, J.E.,
1298 2013. Martian Fluvial Conglomerates at Gale Crater. *Science* 340, 1068–1072.
1299 <https://doi.org/10.1126/science.1237317>
- 1300 Williams, R.M.E., Irwin, R.P., Zimbelman, J.R., 2009. Evaluation of paleohydrologic models for
1301 terrestrial inverted channels: Implications for application to martian sinuous ridges.
1302 *Geomorphology* 107, 300–315. <https://doi.org/10.1016/j.geomorph.2008.12.015>
- 1303 Wyrick, D., 2004. Distribution, morphology, and origins of Martian pit crater chains. *J. Geophys. Res.*
1304 109. <https://doi.org/10.1029/2004JE002240>
- 1305 Xiao, Z., Zeng, Z., Ding, N., Molaro, J., 2013. Mass wasting features on the Moon – how active is the
1306 lunar surface? *Earth Planet. Sci. Lett.* 376, 1–11. <https://doi.org/10.1016/j.epsl.2013.06.015>
- 1307 Zharkova, A.Yu., Kreslavsky, M.A., Head, J.W., Kokhanov, A.A., 2020. Regolith textures on Mercury:
1308 Comparison with the Moon. *Icarus* 351, 113945.
1309 <https://doi.org/10.1016/j.icarus.2020.113945>
- 1310 Zimbelman, J.R., Foroutan, M., 2020. Dingo Gap: Curiosity Went Up a Small Transverse Aeolian Ridge
1311 and Came Down a Megaripple. *J. Geophys. Res. Planets* 125.
1312 <https://doi.org/10.1029/2020JE006489>
- 1313



1314

1315 Figure 1: Aeolian planetary landforms. a) Dark Dunefield on the floor of a 35-km-diameter crater in
1316 Aonia Terra on Mars (sunlight from the left), CaSSIS image MY36_015406_006_0, credit
1317 ESA/Roscosmos/Unibe. b) Large ripples (spacing 2-2.5 m) superposed by smaller impact ripples on

1318 the secondary lee slope of Namib Dune in Gale Crater on Mars (sunlight from the left). Mosaic of MSL
1319 Mastcam images from sol 1192 (Ewing et al., 2017), credit NASA/JPL-Caltech/Malin Space Science
1320 Systems. c) Transverse aeolian ridges (TARs) on the floor of a 17-km-diameter crater in Margaritifer
1321 Terra on Mars (sunlight from the left), CaSSIS image MY36_015406_006_0, credit
1322 ESA/Roscosmos/Unibe. (d) Cassini Synthetic Aperture radar image of the Shangri-La Sand Sea on
1323 Titan (PIA20710). Image credit NASA/JPL-Caltech/ASI. (e) Yardangs and an inverted channel in Aeolis
1324 Mensae region of Mars (sunlight from the right), CaSSIS image MY34_005683_188_2, credit
1325 ESA/Roscosmos/Unibe. (f) Dust Devil in Amazonis Planitia on Mars (sunlight from the left), CTX image
1326 D02_028082_2155. Credit NASA/JPL/MSSS. North is up in all images apart from (b).

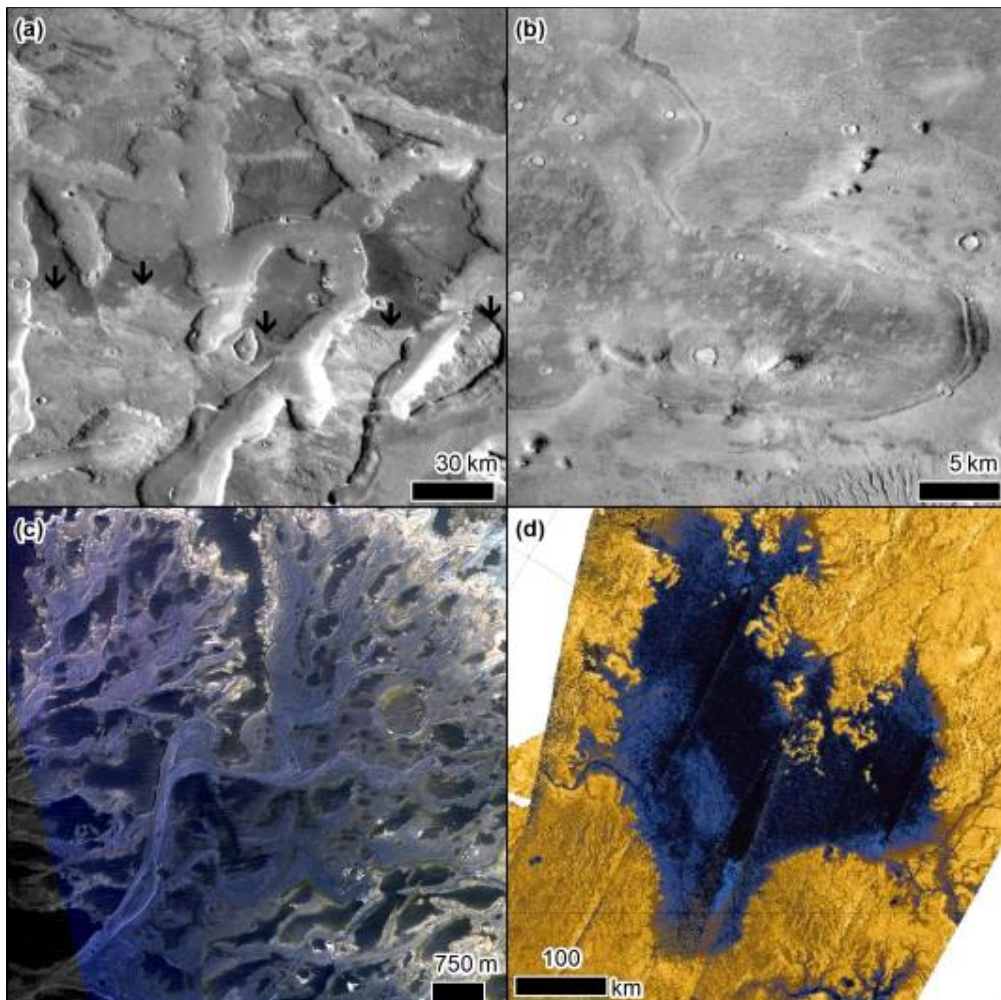


1327

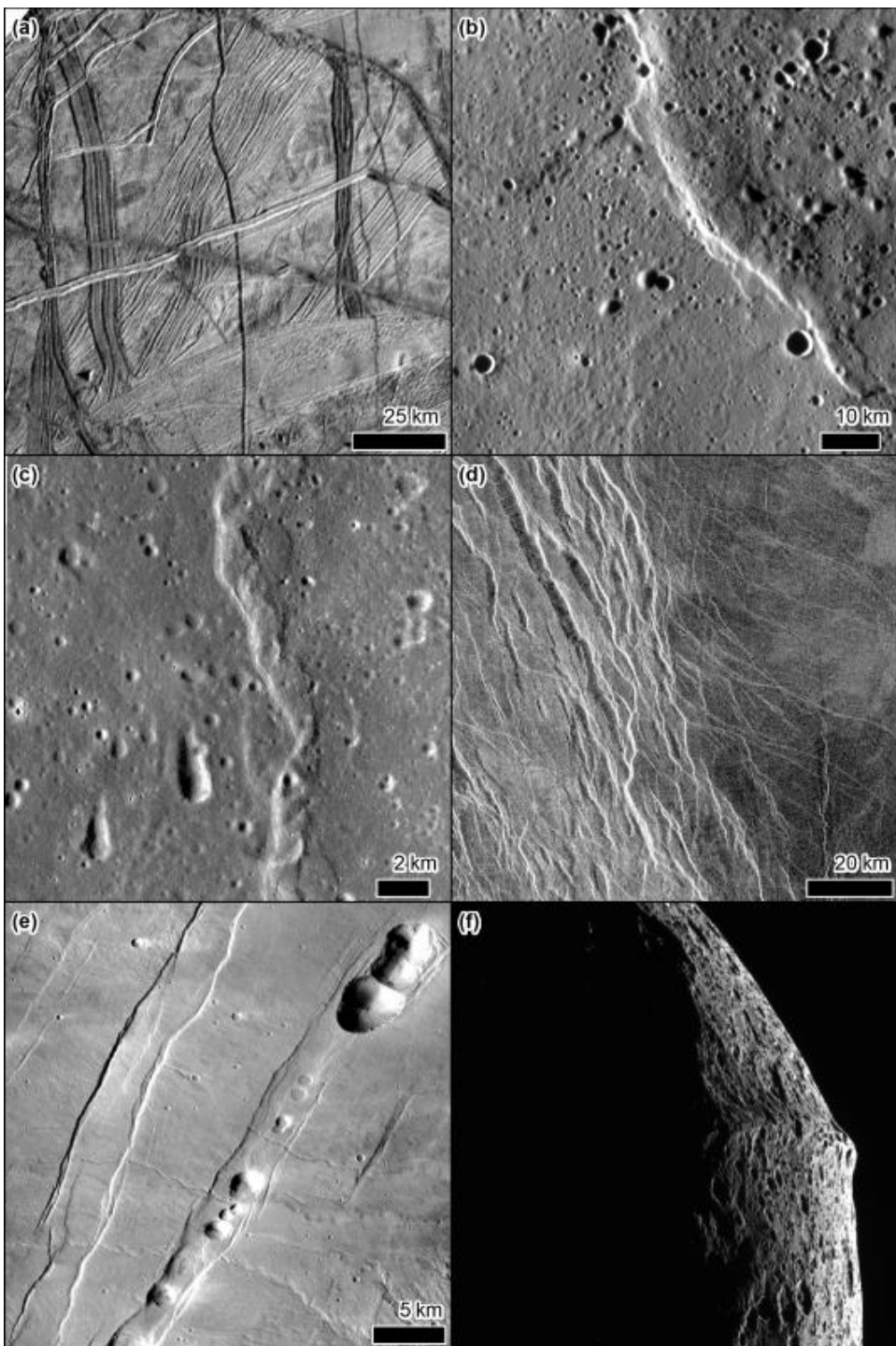
1328 Figure 2: Fluvial planetary landforms. a) Evros Vallis, a valley network in Sinus Sabaeus region of Mars
 1329 (sunlight from the left). The image is the Day IR THEMIS controlled mosaic available from the USGS.
 1330 b) A synthetic aperture radar image of valleys near Titan's south pole taken by the Cassini spacecraft
 1331 image reference PIA10219, credit NASA/JPL-Caltech/ASI. c) Baetis Chaos leading north into Maja

1332 Valles outflow channel on Mars (sunlight from the left). The image is the Day IR THEMIS controlled
1333 mosaic available from the USGS. d) Chaos terrain on Europa near Agenor Linea (sunlight from the
1334 right) taken by Galileo, image reference PIA23873, credit NASA/JPL-Caltech/SETI Institute. e) Two
1335 false-colour images of gullies on Mars (sunlight from the left in both): left Crater in Terra Cimmeria
1336 HiRISE image PSP_004019_1420 and right Gasa Crater, HiRISE image PSP_003939_1420, credit
1337 NASA/JPL/UofA. f) Recurring Slope Lineae in Palikir Crater (sunlight from the left), HiRISE image
1338 ESP_031102_1380, credit NASA/JPL/UofA. North is up in all images.

1339

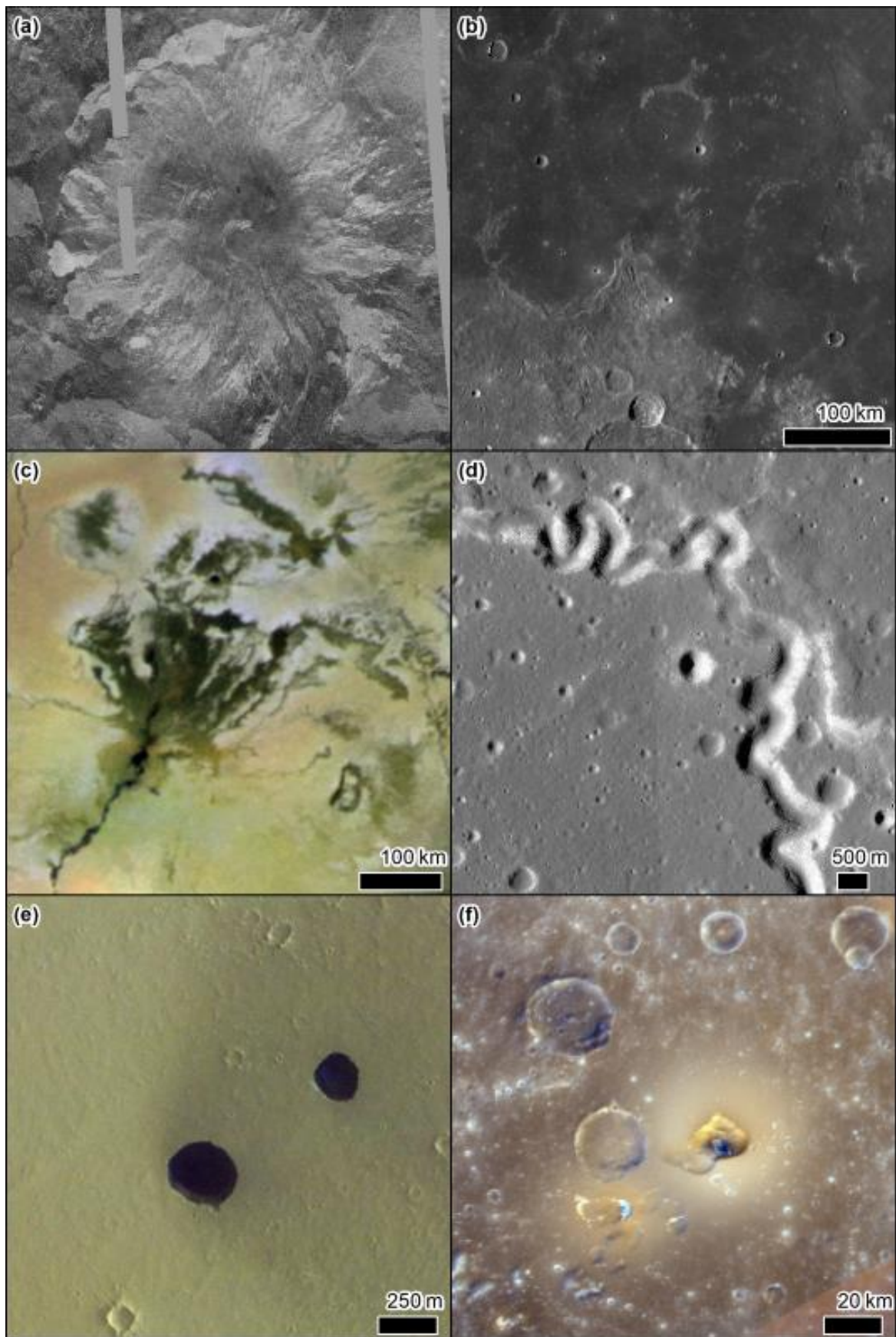


1340
1341 Figure 3: Coastal and lacustrine planetary landforms. a) Albedo contrast (black arrows) interpreted as
1342 a shoreline of a former northern ocean on Mars as seen in the Day IR THEMIS controlled mosaic
1343 available from the USGS (sunlight from the left). b) Lobate features interpreted to be tsunami runup
1344 deposits originating from an impact into a former northern ocean (sunlight from the left). CTX image
1345 P17_007835_2249, credit NASA/JPL/MSSS. c) CaSSIS false colour image of the inverted distributary
1346 channel systems within Eberswalde Crater on Mars, interpreted to be eroded remnants of a delta
1347 that formed within a lake in the crater (sunlight from bottom-right). CaSSIS images
1348 MY34_004384_206_1 and MY34_004384_206_2, credit ESA/Roscosmos/Unibe. d) Cassini false-
1349 colour radar image of Ligeia Mare, the second largest known sea of liquid hydrocarbons on Titan,
1350 credit: NASA/ESA/T. Cornet. North is up in all images.



1351

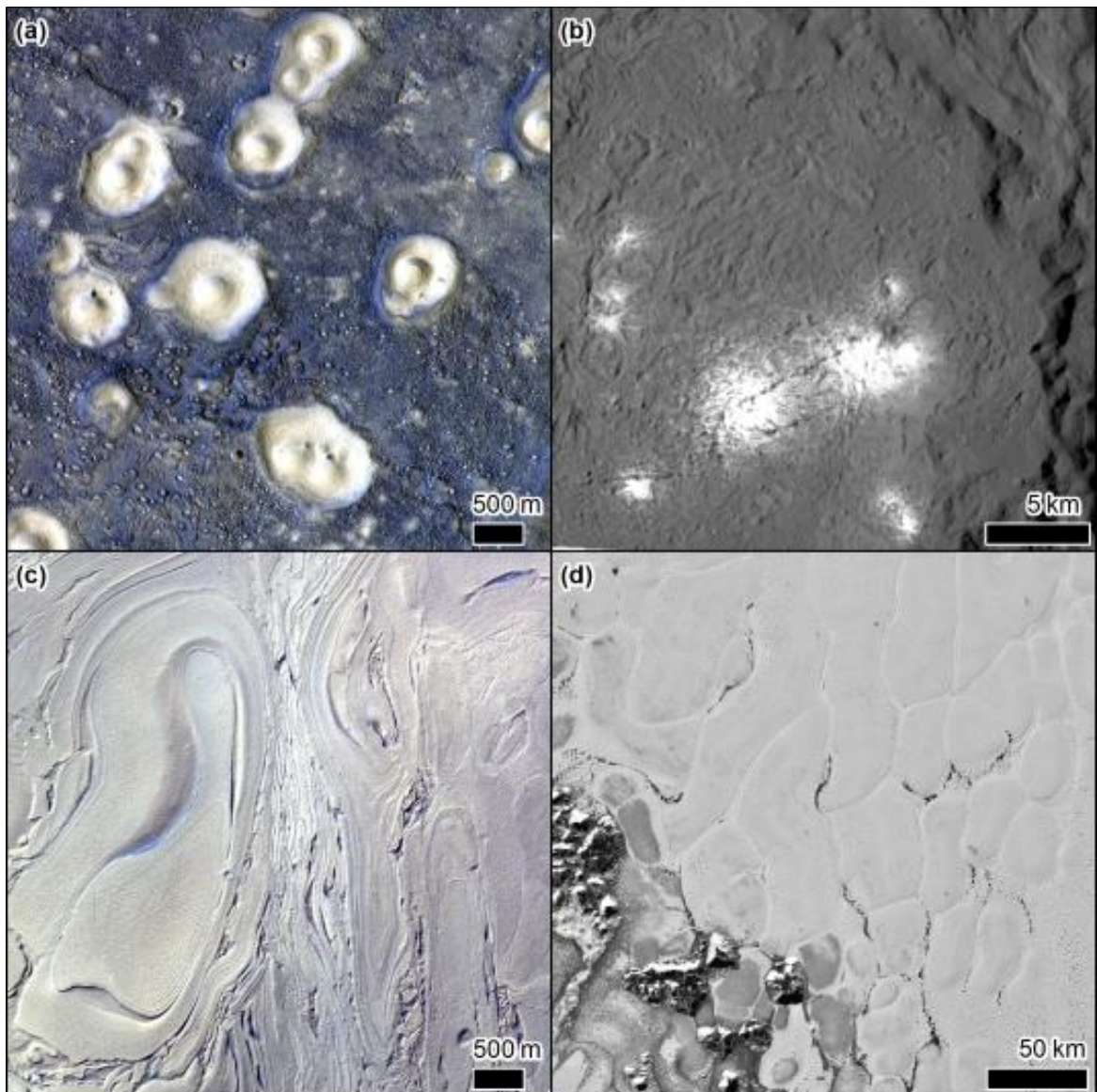
1352 Figure 4: Tectonic planetary landforms. a) The surface of Europa divided into “plates” criss-crossed by
 1353 fractures containing internal parallel ridges. Galileo SSI image 4700R, credit NASA/JPL-Caltech/SETI
 1354 Institute. b) A lobate scarp on Mercury (sunlight from the left), MESSENGER MDIS NAC image
 1355 EN1014447282M, credit NASA/Johns Hopkins University Applied Physics Laboratory/Carnegie
 1356 Institution of Washington. c) Wrinkle ridge on the Moon (sunlight from the left), LROC NAC images
 1357 M181023296 and M104376385, credit NASA/GSFC/ASU. d) Graben on Venus, extract of the Venus
 1358 Magellan SAR FMAP Left Look Global Mosaic from the USGS. e) Graben and pit chains on Mars
 1359 (sunlight from the left), CTX image B18_016700_2167, credit NASA/JPL/MSSS. f) Limb image of
 1360 Iapetus, showing the 20 km high equatorial ridge, taken by Cassini N1568094172_2. North is up in all
 1361 images except f.



1362

1363 Figure 5: Volcanic planetary landforms. a) Tuulikki Mons a shield volcano on Venus, extract of the
1364 Venus Magellan SAR FMAP Left Look Global Mosaic from the USGS. b) The lunar maria with portions

1365 of embayed impact crater rims visible and the contact with the highlands towards the bottom left
1366 (sunlight from the left). LORC WAC global mosaic made available by the USGS. c) Volund dark
1367 volcanic field on Io (Veeder et al., 2009) using the USGS Io basemap combining Voyager and Galileo
1368 images. d) Sinuous rilles on the Moon (sunlight from the left), LROC NAC image M1157998924, credit
1369 NASA/GSFC/ASU. e) Skylights on Mars (sunlight from the top-right), with the east-facing walls barely
1370 visible. CaSSIS false colour image MY36_015278_162_0, credit: ESA/Roscosmos/Unibe. f) Agwo
1371 Facula on Mercury, where the central vent is surrounded by smooth deposits with an orange
1372 coloration in the MDIS enhanced colour mosaic overlain by MDIS WAC image EW1012888774 (where
1373 sunlight is from the bottom), credit NASA/Johns Hopkins University Applied Physics
1374 Laboratory/Carnegie Institution of Washington. North is up in all images.

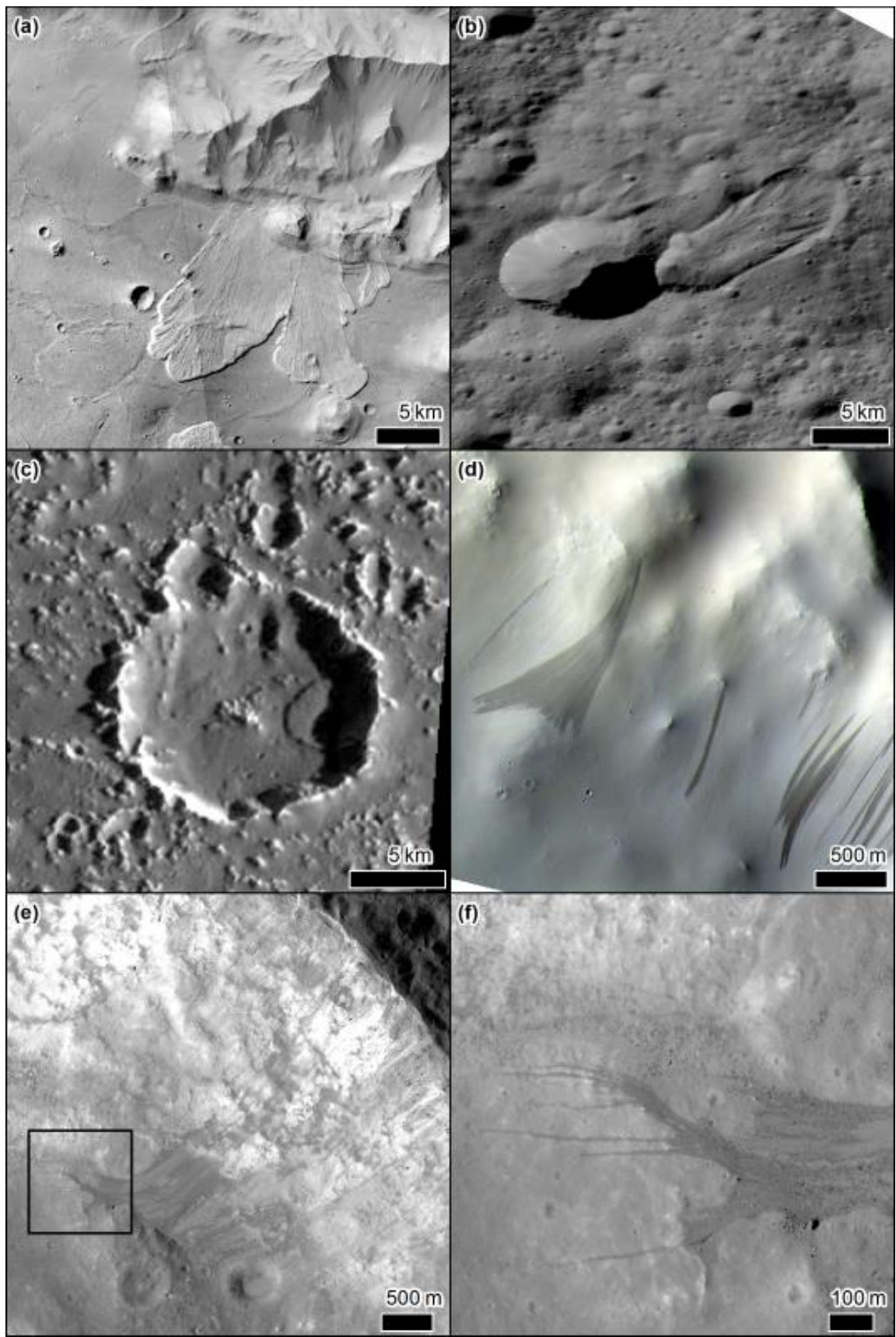


1375
1376 Figure 6: Sedimentary volcanism and cryo-volcanic landforms. a) Pitted cones interpreted to result
1377 from mud volcanism in Acidalia Planitia on Mars (sunlight from the top-right). CaSSIS image
1378 MY35_009227_048_0 credit: ESA/Roscosmos/Unibe. b) Bright faculae in Occator Crater on Ceres
1379 interpreted to be salt deposits resulting from cryovolcanism (sunlight from the right). DAWN framing
1380 camera image FC21B0070808_16169044543F6C, credit NASA/JPL-Caltech/UCLA/MPS/DLR/IDA. c)
1381 The enigmatic banded terrain on the floor of Hellas Basin on Mars (sunlight from the left). CaSSIS
1382 image MY36_015427_317_0 credit: ESA/Roscosmos/Unibe. d) The mysterious cellular structure of

1383 Sputnik Planitia on Pluto (sunlight from the top), image New Horizons global mosaic from the USGS.

1384 North is up in all images.

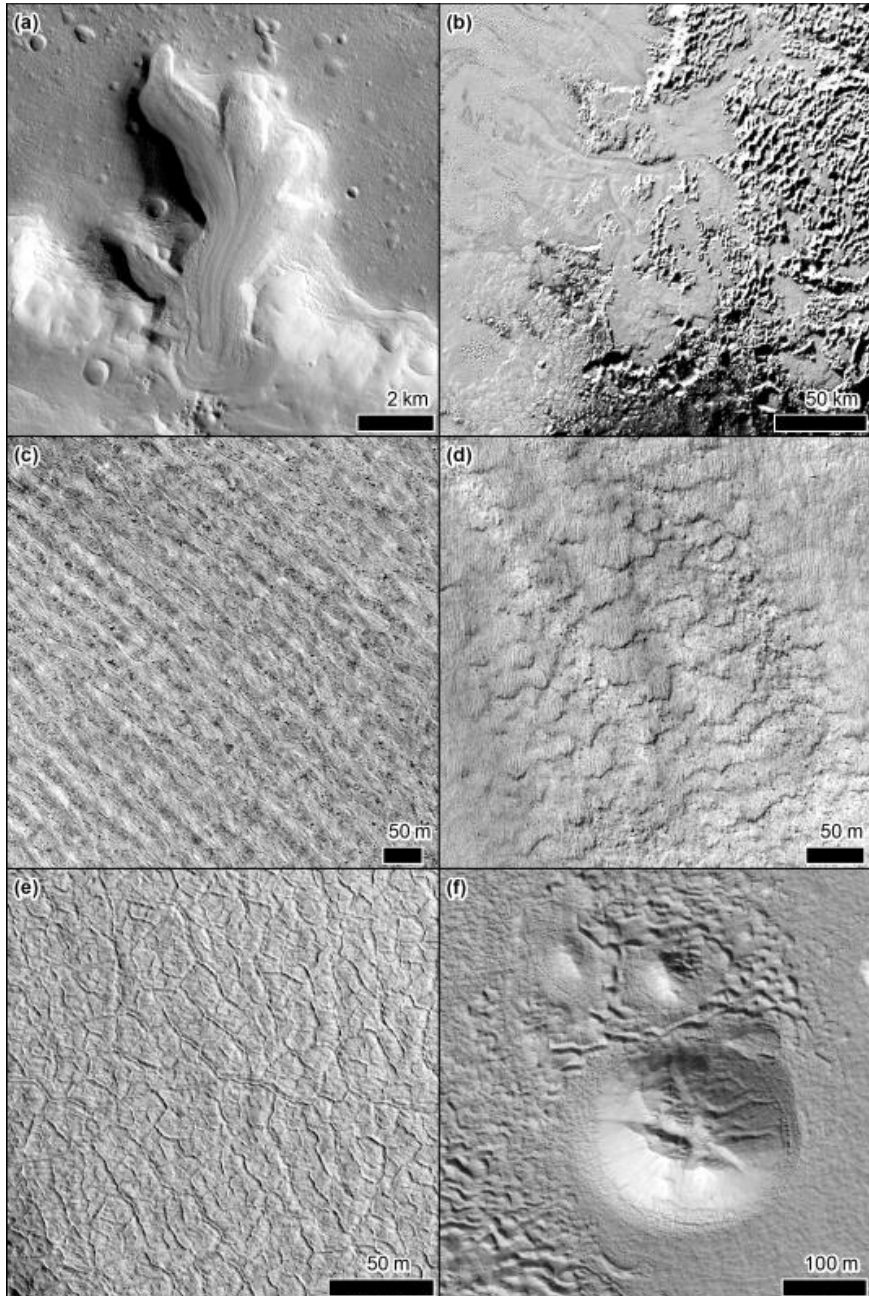
1385



1386
1387
1388
1389
1390

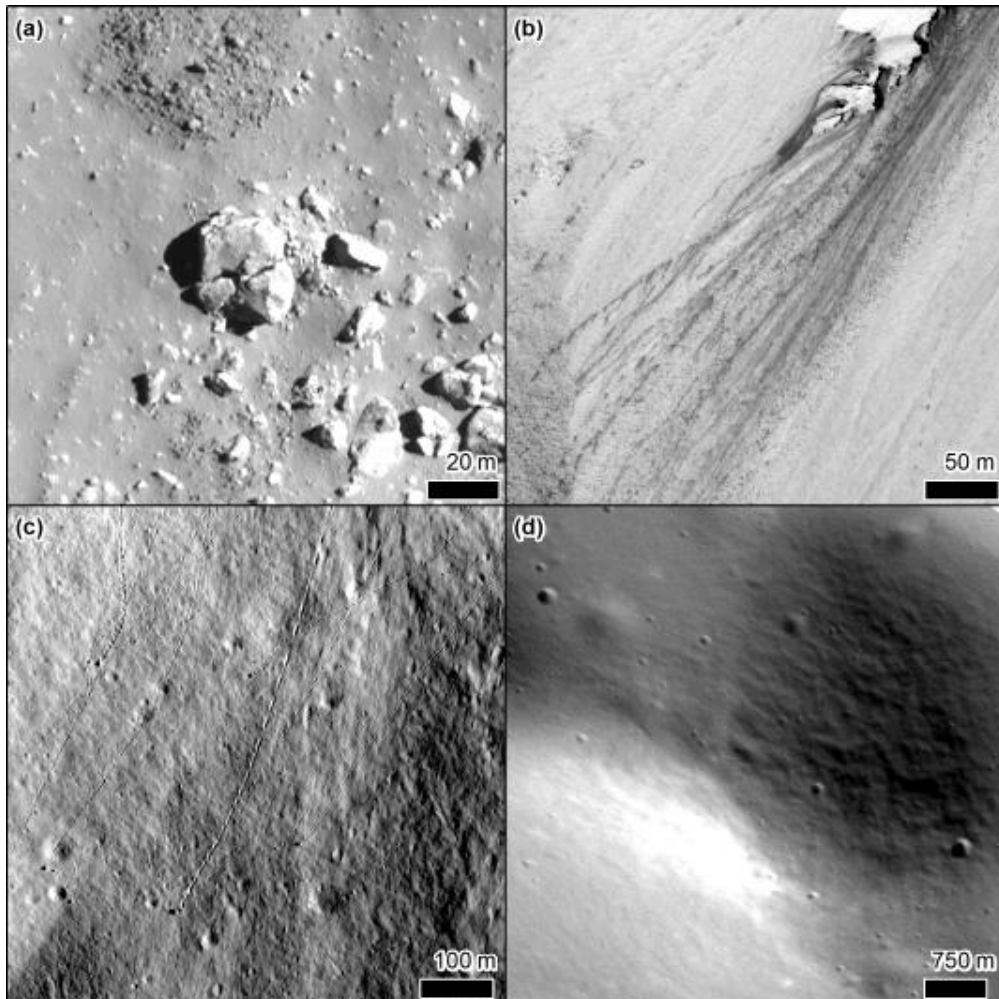
Figure 7: Planetary Mass Movements. a) Landslides in Valles Marineris on Mars (sunlight from the left), CTX images D20_034988_1669, G19_025850_1688, credit NASA/JPL/MSSS. b) Landslide on Ceres (sunlight from the bottom), DAWN FC FC21A0061028_16091125549F1D. c) Landslide on Callisto (sunlight from the right), Galileo SSI image 2840R, credit NASA/JPL-Caltech/SETI Institute. d)

1391 Slope Streaks on Mars (sunlight from the left), CaSSIS image MY36_015392_011_0 credit:
1392 ESA/Roscosmos/Unibe. e) Granular flows in Kepler Crater on the Moon (sunlight from the left), LROC
1393 NAC images credit: NASA/GSFC/ASU. f) Zoom in on the termini of the granular flows in panel e. North
1394 is up in all images.

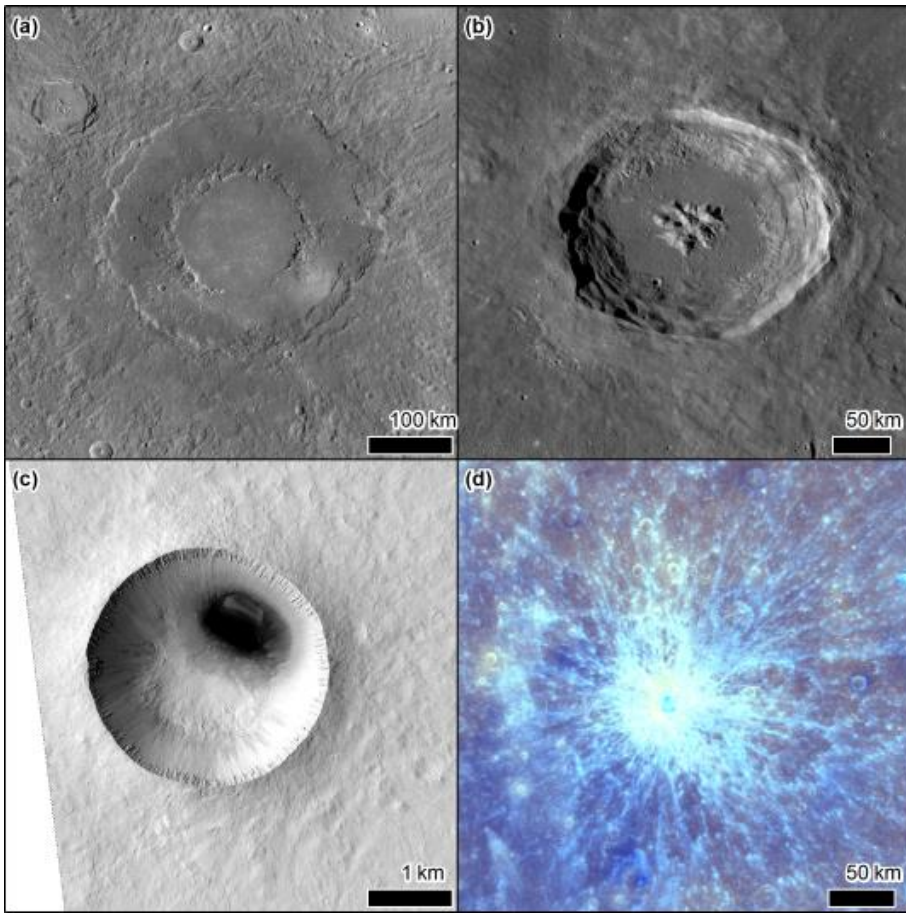


1395
1396 Figure 8: Planetary glacial and periglacial landforms. a) Debris covered glacier on Mars (sunlight from
1397 the left), CTX Image B05_011776_2208, credit NASA/JPL/MSSS. b) Glacial flows on Pluto imaged by
1398 New Horizons (sunlight from top-left), taken from the Global Mosaic available from the USGS. c)
1399 Linear arrangements of boulder propagating downslope interpreted to be sorted patterned ground
1400 on an impact crater wall in the high northern latitudes on Mars (sunlight from top-left), HiRISE image
1401 PSP_009580_2485, credit NASA/JPL/UofA. d) Lobate forms on the wall of an impact crater on Mars
1402 interpreted to be solifluction lobes (sunlight from the left), HiRISE image ESP_023679_1365, credit
1403 NASA/JPL/UofA. e) Polygonal fractured ground where the polygon boundaries are raised as single or
1404 double ridges, termed low centres polygons (sunlight from bottom-left), HiRISE image

1405 PSP_005821_1095 credit NASA/JPL/UofA. f) A mound with a fractured summit near Moreaux Crater
1406 on Mars interpreted to be a pingo (sunlight from bottom-left), HiRISE image ESP_058140_2225 credit
1407 NASA/JPL/UofA. North is up in all images.

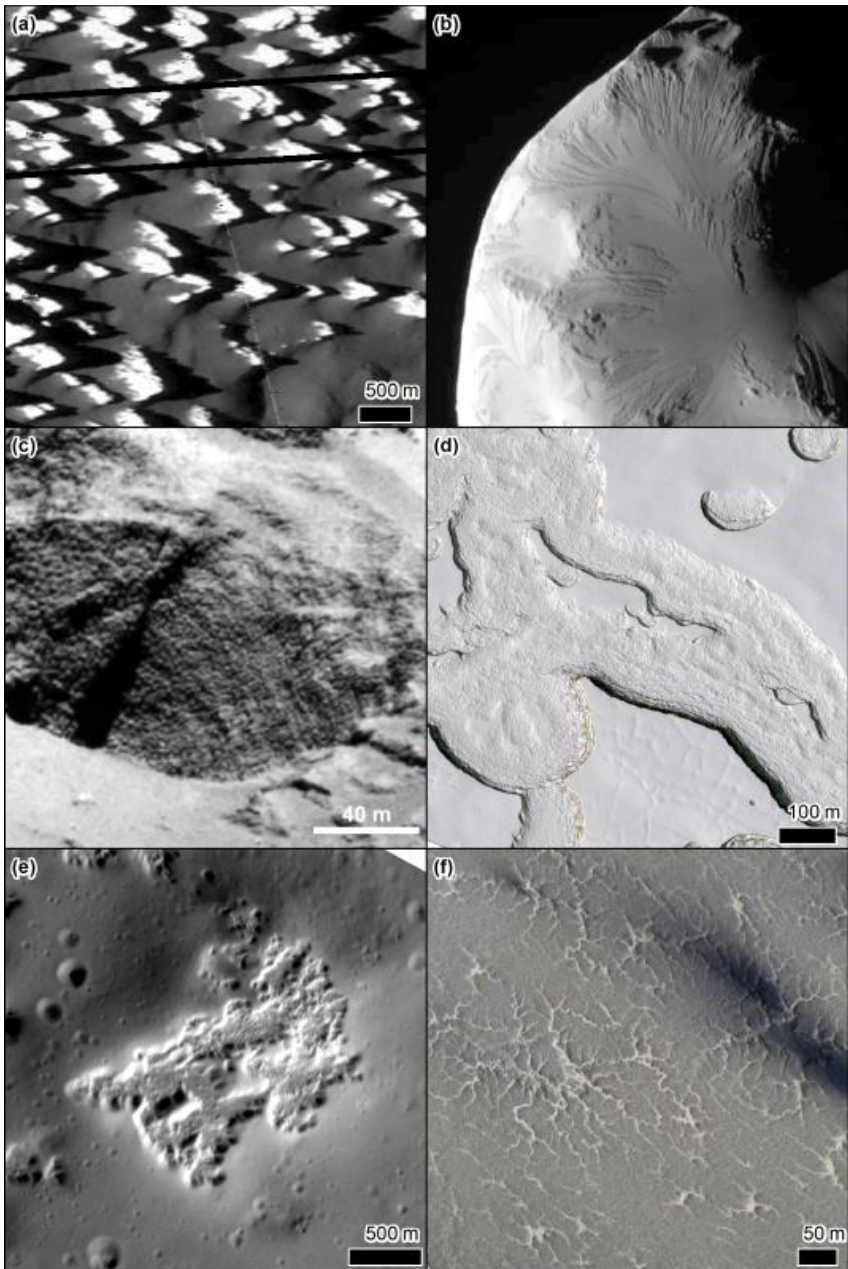


1408
1409 Figure 9: Weathering on planetary surfaces. a) Fractured rocks around Byrgius A Crater on the Moon
1410 (sunlight from the right), LROC NAC image M175698856LE, credit NASA/GSFC/ASU. b) Tracks and low
1411 albedo "ejecta" left by recent rockfalls on a crater wall on Mars (sunlight from the left), HiRISE image
1412 PSP_004110_1640, credit NASA/JPL/UofA. c) Multiple rocks which have left depressions behind them
1413 while rolling and bouncing over the lunar surface (sunlight from the right), LROC NAC image
1414 M1198659818LE, credit NASA/GSFC/ASU. d) Undulating, irregular surface texture on Mercury
1415 (sunlight from the bottom-left), termed "Elephant hide" (Zharkova et al., 2020) MDIS NAC image
1416 EN1042186062M, credit NASA/Johns Hopkins University Applied Physics Laboratory/Carnegie
1417 Institution of Washington. North is up in all images.



1418

1419 Figure 10: Impact craters on Planetary bodies. a) Rachmanioff, an impact basin on Mercury, with
 1420 noticeable multiple rings (sunlight from the right), MDIS global BDR mosaic, credit NASA/Johns
 1421 Hopkins University Applied Physics Laboratory/Carnegie Institution of Washington. b) Arstillus, a
 1422 complex crater with central peak and wall terraces on the Moon (sunlight from the left), LRO global
 1423 WAC mosaic, credit NASA/GSFC/Arizona State University. c) ~ 2km diameter simple crater on the
 1424 floor of Pasteur Crater on Mars (sunlight from the left), HiRISE image ESP_045152_2000, credit
 1425 NASA/JPL/UofA. d) Petipa, an impact crater with rayed ejecta on Mercury (sunlight from overhead),
 1426 MDIS global enhanced color mosaic, credit NASA/Johns Hopkins University Applied Physics
 1427 Laboratory/Carnegie Institution of Washington. North is up in all images.



1428

1429 Figure 11: Sublimation dominated landscapes and landforms. a) Pinnacle terrain on Callisto Galileo
 1430 (sunlight from the left) SSI image 5214R, credit NASA/JPL-Caltech/SETI Institute. b) Image of the
 1431 surface of Helene a moon of Saturn (sunlight from the left) taken by the Cassini spacecraft image
 1432 reference N1687119876_1, credit NASA/JPL-Caltech/ASI, scene is about 30 km across. c) Oblique
 1433 image of the wall of a steep pit revealing internal structure (sunlight from the left), on comet
 1434 67P/Churyumov–Gerasimenko taken by the OSIRIS narrow-angle camera, credit ESA/Rosetta/MPS
 1435 for OSIRIS Team MPS/UPD/LAM/IAA/SSO/INTA/UPM/DASP/IDA. d) Siss cheese terrain in the CO₂ ice
 1436 on the south polar cap of Mars (sunlight from the bottom-left), HiRISE image ESP_057828_0930,
 1437 credit NASA/JPL/UofA. e) Hollows on Mercury (sunlight from the bottom-right), MDIS NAC image
 1438 EN1042186062M, credit NASA/Johns Hopkins University Applied Physics Laboratory/Carnegie
 1439 Institution of Washington. f) Spiders on Mars (sunlight from the top-right), where the dark marks are
 1440 dust fans deposited by seasonal jets, HiRISE image ESP_055604_0930, credit NASA/JPL/UofA.